Contrasting roles of cytochrome P450s in amitraz and chlorfenapyr resistance in the crop pest *Tetranychus urticae*

Marilou Vandenhole[1§], Xueping Lu[1§], Dimitra Tsakireli[2,3§], Catherine Mermans[1], Sander De Rouck[1], Berdien De Beer[1], Eba Simma[4], Spiros A. Pergantis[5], Wim Jonckheere[1], John Vontas[2,3], Thomas Van Leeuwen[1*]

[1]Department of Plants and Crops, Faculty of Bioscience Engineering, Ghent University, Coupure links 653, Ghent, Belgium.

[2] Laboratory of Pesticide Science, Department of Crop Science, Agricultural University of Athens, 75 Iera Odos Street, GR-11855 Athens, Greece

[3] Institute of Molecular Biology and Biotechnology, Foundation for Research and Technology Hellas, GR-700 13 Heraklion, Crete, Greece

[4] Department of Biology, College of Natural Sciences, Jimma University, Jimma, Ethiopia.

[5] Environmental Chemical Processes Laboratory, Department of Chemistry, University of Crete, Voutes Campus, 70013, Heraklion, Crete, Greece

[§]These authors contributed equally

*Corresponding author: thomas.vanleeuwen@ugent.be

Key words: gene regulation, acaricide resistance, detoxification, genetic mapping, mitochondrial uncouplers, octopamine receptor, spider mite

Abstract

The molecular mechanisms of amitraz and chlorfenapyr resistance remain only poorly understood for major agricultural pests and vectors of human diseases. This study focusses on a multi-resistant field strain of the crop pest *Tetranychus urticae*, which could be readily selected in the laboratory to high levels of amitraz and chlorfenapyr resistance. Toxicity experiments using tralopyril, the active toxophore of chlorfenapyr, suggested decreased activation as a likely mechanism underlying resistance. Starting from the same parental strain, transcriptome profiling revealed that a cluster of detoxifying genes was upregulated after amitraz selection, but unexpectedly downregulated after chlorfenapyr selection. Further functional validation associated the upregulation of CYP392A16 with amitraz metabolism and the downregulation of CYP392D8 with reduced activation of chlorfenapyr to tralopyril. Genetic mapping (QTL analysis by BSA) was conducted in an attempt to unravel the genetic mechanisms of expression variation and resistance. This revealed that chlorfenapyr resistance was associated with a single QTL, while 3 QTLs were uncovered for amitraz resistance. Together with the observed contrasting gene expression patterns, we argue that transcriptional regulators most likely underly the distinct expression profiles associated with resistance, but these await further functional validation.

1 Introduction

The two-spotted spider mite, *Tetranychus urticae* Koch (Acari: Tetranychidae), is a cosmopolitan agricultural pest known for its exceptionally wide host range (Grbić et al., 2011). This pest can feed on over 1100 plant species from more than 140 different families, including some well-known toxin-producing plants (Migeon et al., 2010). With the potential to severely infest more than 150 annual and perennial crops and ornamental plant species, *T. urticae* poses a significant economic threat in greenhouses and field crops (Grbić et al., 2011; Van Leeuwen et al., 2010). Synthetic acaricides play a crucial role in the management of *T. urticae* in many agronomic crops due to their effectiveness, ease of use, and low cost (Damalas, 2009; Van Leeuwen et al., 2015). Unfortunately, *T. urticae* is notorious for its ability to quickly develop resistance to a variety of acaricides due to its high fecundity, rapid development and arrhenotokous reproduction (De Rouck et al., 2023; Van Leeuwen and Dermauw, 2016). According to the Arthropod Pesticide Resistance Database (http://www.pesticideresistance.org), there have been 432 recorded cases of resistance to 96 active ingredients for *T. urticae*, including major groups of currently used acaricides (David and John, 2023; De Rouck et al., 2023; Riga et al., 2017; Sparks and Nauen, 2015; Van Leeuwen and Dermauw, 2016). The rising cost of discovery, development, and registration have made the agro-industry more reluctant to develop new crop protection chemicals (Sparks, 2013). Therefore, there is a pressing need for improved evidence-based integrated resistance managements (IRM), including appropriate application of existing acaricides. One alternative approach to the current use-and-dispose method might be to employ negative cross-resistance (NCR) strategies to manage organisms that already show resistance against various compounds. NCR describes a phenotype in which a strain has developed resistance to one pesticide but shows greater sensitivity to some pesticides. Recent studies and reviews have emphasized the potential of use of pro-pesticides for resistance management, as they show most cases of NCR (David, 2021). Amongst these pro-pesticides, chlorfenapyr is particularly noteworthy as there are numerous cases of NCR across arthropods (David, 2021; Leonard, 2000; Nicastro et al., 2013).

Chlorfenapyr is a broad-spectrum pyrrole pesticide belonging to IRAC Group 13 and is mainly used for termite control and crop protection against a variety of insect and mite pests (Lovell et al., 1990; Pimprale et al., 1997; Sheppard and Joyce, 1998; Sparks and Nauen, 2015). Chlorfenapyr is a pro-acaricide which needs oxidative removal of the N-ethoxymethyl group *in vivo* to activate its pesticidal potential and form the toxic metabolite tralopyril. Tralopyril is a

lipophilic compound with weakly acidic properties due to the presence of an acidic proton in the pyrrole ring and thus exhibits protonophoric activities. It acts by transporting protons across the mitochondrial membrane, thereby interfering with mitochondrial oxidative phosphorylation. This disruption of ATP synthesis leads to cell dysfunction and ultimately the demise of the target organism (Black et al., 1994; Raghavendra et al., 2011b; Terada, 1990). Another important but less studied pro-acaricide is amitraz. Amitraz is a formamidine pro-pesticide belonging to IRAC Group 19 (Hollingworth, 1976; Sparks et al., 2021). Amitraz can act as an agonist by stimulating the β-adrenergic-like octopamine receptors (βAOR), but its active metabolite, DPMF (N^2-(2,4-dimethylphenyl)-N^1–methylformamidine), is an even stronger agonist (Cai et al., 2023; Kita et al., 2017; Takata et al., 2020). Important to note is the observed strong connection from toxicity bioassays between chlorfenapyr and amitraz resistance in *T. urticae* strains (Aguilar-Medel et al., 2011; AI-Antary et al., 2012; Herron and Rophail, 2003; Simma et al., 2020; Van Leeuwen et al., 2005, 2004). This observation raises the question of whether a "hitchhiking effect" is at play, wherein two closely linked pesticide resistance genes under one acaricide pressure are simultaneously favored (Kojima and Schaffer, 1967; Smith and Haigh, 1974), or if a single evolved gene provides resistance to more than one molecule (Duarte et al., 2022). The level of connection between chlorfenapyr and amitraz – two compounds with completely different MOAs, targeting respiration and neural functions respectively – could heighten concerns for pest resistance management. Therefore, understanding the mechanisms behind resistance and cross-resistance would help making informed decisions regarding the optimal use and rotation of pesticides, thereby delaying the evolution of resistance and prolonging their efficacy (Dekeyser, 2005). This might be especially important for chlorfenapyr, that is currently also implemented in mosquito control programs as one of the few alternatives (Ngufor et al., 2016; Tchouakui et al., 2023).

Resistance can evolve via two main mechanisms: alterations in the coding sequence of acaricide target genes due to various point mutations leading to decreased acaricide sensitivity (toxicodynamic resistance), or changes in factors affecting absorption, excretion, distribution and metabolism, impacting the overall effectiveness of the acaricide (toxicokinetic resistance) (De Rouck et al., 2023; Feyereisen et al., 2015). Interestingly, a recent study has shown that resistance against pro-insecticides was mediated by downregulation of detoxification enzymes involved in the activation (Vlogiannitis et al., 2021). Although only relatively few studies have investigated chlorfenapyr resistance mechanisms in spider mites, multiple potential mechanisms have been described based on synergist and/or total enzyme assays. These include

metabolic detoxification mediated by carboxyl/cholinesterases, glutathione S-transferases (GSTs) and cytochrome P450s (P450s), as well as decreased cuticular penetration (Li et al., 2005; Van Leeuwen et al., 2006, 2004). Moreover, the induction of P450 activity by barbital and geraniol has been shown to increase chlorfenapyr tolerance in *T. urticae*, possibly through increased detoxification (Van Pottelberge et al., 2008). However, those mechanisms can only explain a part of the resistant phenotype, and the precise underlying mechanisms remain largely unknown. In any case, it is likely that metabolic resistance mechanisms are at play because uncouplers like chlorfenapyr do not bind to a specific protein (target-site), unlike most insecticides and acaricides. Also for amitraz, the resistance mechanisms in spider mites have remained largely elusive. However, studies on other tick and mite species suggested the involvement of target-site mutations in the octopamine/tyramine (OCT/Tyr) receptors, the β-adrenergic octopamine receptor (βOAR) or its 5' untranslated region (UTR) (Baron et al., 2015; Corley et al., 2013; De Rouck et al., 2023). However, synergist experiments also suggest the involvement of P450s (Chevillon et al., 2007; Ducornez et al., 2005). Nevertheless, amitraz resistance mechanism are despite their importance only poorly studied in mites and ticks. Spider mites like *T. urticae*, with a wealth of available toxicological and genetic tools (De Rouck et al. 2023), might be useful to resolve some of the standing questions in the field for both amitraz and chlorfenapyr (cross-)resistance mechanisms.

A previous screening study identified an Ethiopian field strain of *T. urticae* resistant to both chlorfenapyr and amitraz (Simma et al., 2020). Here, we took advantage of this strain to study the molecular mechanisms of resistance. For this purpose, this strain was further selected in the laboratory with chlorfenapyr and amitraz separately and the phenotypic strength of resistance was quantified. Considering reduced activation as a potential resistance mechanism in chlorfenapyr resistance, also toxicity of the active metabolite tralopyril was assessed. Next, synergist assays were conducted to explore the potential involvement of detoxification enzymes in resistance mechanisms against both acaricides, followed by transcriptome sequencing of parental and selected populations with and without acaricide exposure. Identified candidate P450s were validated *in vitro* via recombinant expression and metabolic assays. We further tried to unravel the genetic complexity of chlorfenapyr/amitraz resistance by genetic mapping via bulked segregant analysis (BSA).

2. Materials and methods

2.1 Chemicals used

The acaricides used for strain selection and toxicity bioassays were a commercial formulation of amitraz (Mitac; 20 g a.i. L^{-1} EC) from Arysta Life Science (Ethiopia) and chlorfenapyr (240 g a.i. L^{-1} SC) from BASF (Canada) for experimental use. The analytical standard of tralopyril (CAS 122454-29-9) was purchased from LGC (UK). Technical grade amitraz and chlorfenapyr were purchased from Sigma Aldrich (USA). The synergists diethyl maleate (DEM) and piperonyl butoxide (PBO) were of analytical grade and purchased from Sigma-Aldrich (Belgium), S,S,S-tributyl phosphorotrithioate (DEF) was purchased from Chemservice (USA).

2.2 Spider mite strains

Two *T. urticae* strains originally collected from Ethiopia were used: Jimma Wild and Holeta-2. Jimma Wild (abbreviation JW) was collected in 2018 from wild ornamentals in Jimma, while the Holeta-2 parental strain (abbreviation HP) was collected from greenhouse strawberry plants in Holeta in 2019 (Simma et al., 2020). HP was highly resistant to fenbutatin oxide, amitraz and fenpyroximate, but also moderately resistant to chlorfenapyr (Simma et al., 2020). The HP strain was used to set-up laboratory-selection with both chlorfenapyr and amitraz, giving rise to the resistant strains HPC and HPA, respectively. The strains were maintained on sprayed kidney bean plants (*Phaseolus vulgaris* var. Prelude) at a constant selection pressure of 500 mg L^{-1} chlorfenapyr and 1000 mg L^{-1} amitraz. JW, which was susceptible to both chlorfenapyr and amitraz (Simma et al., 2020), was reared on untreated kidney bean plants. Additionally, two laboratory strains were used: the susceptible reference strain London (abbreviation LON) (Grbić et al., 2011), and the inbred strain ROS-ITi which originated from the ROS-IT strain after 7-8 generations of consecutive mother-son mating (De Beer et al., 2022a; Kurlovs et al., 2022). ROS-ITi was highly susceptible to most tested acaricidal compounds, with the exception of dicofol (Kurlovs et al., 2022). Both LON and ROS-ITi were maintained on untreated bean plants. All strains were kept in climatically controlled rooms at 25 ± 1 °C, 60% relative humidity (RH), 16:8 h light:dark photoperiod. Fresh potted bean plants were offered when needed.

2.3 Toxicity bioassays

Full dose-response adulticidal toxicity bioassays were performed as described previously (Khajehali et al., 2011). Briefly, 20-30 adult female mites were transferred to the upper side of 9 cm^2 square bean leaf discs placed on wet cotton wool. The acaricides amitraz and chlorfenapyr were diluted with water and the technical standard tralopyril was formulated in a mixture of N,N-dimethylformamide (DMF) and alkyl-aryl polyglycol ether (emulsifier W) (3:1 w:w), and

subsequently 100-fold diluted with water to form a stock solution. To determine the lethal concentration 50 (LC_{50}), a minimum of five concentrations was tested in four replicates, along with blank controls that were sprayed with deionized water or a blank formulation (1/100 dilution of mix of DMF and emulsifier W) for tralopyril bioassays. Mites were sprayed with 0.8 ml of serial acaricide dilutions at 1 bar pressure using a Cornelis spray tower resulting in a homogenous spray film of 2.00 ± 0.05 mg cm^{-2} aqueous acaricide deposit (Van Laecke and Degheele, 1993). Mortality was scored after 72 h and mites were scored as "dead" if they did not move one body length within 10 seconds after being prodded with a fine brush. Dose-response relationships (LC_{50} and 95% confidence interval (CI)) were calculated from probit regression using PoloPlus software (LeOra software, USA).

2.4 Determining the mode of inheritance of chlorfenapyr resistance

To estimate the degree of dominance and to identify potential maternal inheritance of chlorfenapyr resistance, mites of the susceptible LON and chlorfenapyr resistant HPC strain were reciprocally crossed to produce hybrid F_1 females, as previously described (Van Pottelberge et al., 2009), and used for toxicity bioassays as described above. Dominance was determined using the Stone formula (Stone, 1968); dominance (D) is given by $D = \frac{2X_2 - X_1 - X_3}{X_1 - X_3}$, where X_1 = log LC_{50} of the resistant strain (HPC), X_2 = log LC_{50} of the F_1 females (HPC ♀ × LON ♂ or LON ♀ × HPC ♂) and X_3 = log LC_{50} of the susceptible strain (LON). The number of genes associated with chlorfenapyr resistance was estimated via an F2 backcrossing experiment. F_1 heterozygous unfertilized females from the reciprocal cross (LON ♀ × HPC ♂) were allowed to mate with susceptible LON males on bean leaves for two days. The resulting 1-3 days old F_2 females were then subjected to toxicity bioassays as described above. Single gene inheritance is characterized by a plateau at 50% mortality of the concentration-mortality curves. The expected responses of monogenic F_2 females for each given dose were calculated using the following formula of Georghiou (1969): $c = (0.5)\ W_{\text{LON x HPC}} + (0.5)\ W_{\text{LON}}$, where c is the expected mortality at each given concentration and W is the observed mortality of the F_1 LON x HPC and parental LON genotypes at each given concentration. The dose-response curves (Abbott corrected mortality (Abbott, 1987)) were plotted using Sigmaplot (v.14.5) (Systat, USA). The χ^2 goodness-of-fit test was applied to determine how well the observed responses matched the expected.

2.5 Synergism/antagonism experiments

In order to investigate the potential involvement of metabolic resistance mechanisms, synergist bioassays were performed as described earlier (Snoeck et al., 2017; Van Pottelberge et al., 2009). About 30 young adult female mites were placed on bean leaf discs and sprayed with a non-toxic concentration of 1000 mg L^{-1} PBO, 2000 mg L^{-1} DEM or DEF, dissolved in a mixture (3:1 w:w) of DMF and emulsifier W and subsequently 100-fold diluted with deionized water. Final concentrations for DEF were 300 mg L^{-1} for JW and 500 mg L^{-1} for HPC and HPA, in order to keep mortality below 5-10%. Mites were sprayed with diluted formulations with or without (control) synergists, and subsequently placed in a climatically controlled room as described above. After 24 h, surviving mites were transferred to fresh leaf discs and used in toxicity bioassays with chlorfenapyr or amitraz. Mites sprayed with water served as the control. LC_{50}'s and their 95% CI were determined with PoloPlus software. Synergism ratios (SRs) were calculated by dividing the LC_{50} values from experiments with synergists by LC_{50} values from experiments without synergists.

2.6 Transcriptome analysis

2.6.1 RNA extraction and sequencing

Prior to RNA extraction, both the amitraz- (HPA) and chlorfenapyr-resistant (HPC) strains were placed on unsprayed plants for one generation (± 7 days) ,except for HPAexp and HPCexp strains which experienced continuous exposure. Total RNA was extracted from a pool of 100-120 adult female mites using the Rneasy Mini Kit (Qiagen, Belgium). Four replicates were included for each population: LON, JW, HP, HPA, HPC, HPAexp, and HPCexp. The quality and quantity of the total RNA was analyzed using a DeNovix DS-11 spectrophotometer (DeNovix, USA) and by running an aliquot on a 1% agarose gel. RNA samples were subsequently sent to Macrogen (The Netherlands) for mRNA library construction and sequencing. Libraries were constructed with TruSeq Stranded mRNA Library Preparation Kit (Illumina, USA) and sequenced via Illumina's NovaSeq6000 platform to generate stranded, paired-end reads of 100 bp.

2.6.2 RNA read mapping and PCA

The quality of the RNA reads was assessed using the FastQC software (v.0.11.9) (Andrews, 2010). RNA reads were aligned to the three pseudochromosome assembly of *T. urticae* using the two-pass alignment mode of STAR (v.2.7.9a) with a maximum intron size set to 20 kb (Dobin et al., 2013; Wybouw et al., 2019). After alignment, the BAM files were sorted by

chromosomal coordinate and indexed using SAMtools (v.1.15) (Li et al., 2009). The resulting coordinate-sorted BAM files were used as an input for HTSeq (v.0.11.2) for read-counting on a per-gene basis with the flags "*–stranded yes"* and "*–feature exon"* (Anders et al., 2015). A principal component analysis (PCA) was done based on the resulting read-count files using the R-package DESeq2 (v.1.34.0) in order to investigate transcriptional differences within and between treatment groups (LON, JW, HP, HPA, HPAexp, HPC and HPCexp) (Love et al., 2014). In short, the regularized-logarithm (rlog) transformation function of the DESeq2 package was used to normalize the counts and PlotPCA to calculate and plot the PCA for the 5000 most variable genes across all samples.

2.6.3 K-means clustering analysis

All genes showing differential expression across at least one of the different conditions were clustered using the k-means clustering algorithm. In order to do this, first DESeq2 analysis was performed with a Likelihood Ratio Test (LTR) on the reduced model to analyze all levels of a factor at once. Only genes that had an adjusted *p* value (*p* adj) < 0.001 were filtered out as genes that show significant differences in expression in at least one of the conditions. The normalized read-counts of these genes were transformed into a z-scaled distance dataset using the Pearson method with the "*get_dist*" function within the R-package factoextra (v.1.0.7). This z-scaled dataset was subsequently used as an input for the k-means clustering algorithm using the *"kmeans"* function of the R-package stats (v.4.3.1). The optimal number of 13 clusters was determined using the gap statistic (maximum of number of 25, first max, seed set at 123, nstart set at 25 and the maximum number of iterations set at 50) (Tibshirani et al., 2001). The z-scaled dataset of all genes showing significant differential expression amongst the samples was used to make a heatmap with the R-package pheatmap (v.1.0.12), where rows represent the genes that are grouped according to their respective clusters. For each cluster, plots were made representing the average z-score per treatment group per gene in the cluster, which was thereafter used to calculate the average z-score trend with standard deviation across all genes in the cluster.

The R function enricher from the package clusterProfiler (v.4.2.2) was used for GO enrichment analysis of each cluster of genes. The GO terms for "Biological Processes"(BP) and "Molecular Functions" (MF) were collected based on the *T. urticae* annotation (v.20190125) from the ORCAE database (Sterck et al., 2012). The argument "*pAdjustMethod = 'BH'*" was added to the function in order to perform multiple correction using a Benjamini-Hochberg procedure.

2.6.4 Pairwise differential expression analysis

DESeq2 (v.1.34.0) was used to perform a pairwise differential expression analysis between all strains (LON, JW, HP, HPA, HPC, HPAexp and HPCexp) based on the total read-counts per gene generated by HTSeq (as described in section 2.6.2). Differentially expressed genes (DEGs) were classified as genes with an absolute Log_2 Fold Change ($|Log_2FC|$) > 1 and a Benjamini-Hochberg adjusted *p* value (*p* adj) < 0.05 in the pairwise comparison. A gene expression heatmap for all full-length P450 genes (list published by Kurlovs et al., 2022) was generated using the relative transcript levels (Log_2FC) of the four differential expression comparisons between HP and the derived selected strains (HPA vs HP, HPAexp vs HP, HPC vs HP and HPCexp vs HP) using the pheatmap function in R. P450s were clustered using the Euclidian distance, and P450s that were not differentially expressed ($|Log_2FC| < 1$ and/or *p* adj > 0.05) in all four comparisons were excluded from the heatmap.

2.7 P450 functional expression and metabolism assay

Metabolism assays of P450s with amitraz and chlorfenapyr were performed to investigate their potential role in amitraz/chlorfenapyr resistance or selectivity. The P450 genes *CYP392A16, CYP392A11, CYP392E10, CYP392D8* and *CYP392A1*, which each showed an interesting expression pattern in transcriptomic analysis, were selected to be functionally expressed *in vitro* as described previously (Riga et al., 2014).

2.7.1 P450 HPLC-UV activity assay

Stock concentrations of amitraz (100 % purity, Sigma Aldrich, USA) and DPMF (100% purity, Sigma Aldrich, USA) were prepared and diluted in acetonitrile. Stock concentrations of chlorfenapyr (100 % purity, Sigma Aldrich, USA) were prepared and diluted in methanol. Standard reactions contained a final organic solvent concentration between 2-2.5% (v/v) with 25 µM amitraz, 25 µM DPMF or 20 µM chlorfenapyr, respectively, and 5-25 pmol bacterial membranes from each of the P450s in 100 µl Tris-HCl buffer (0.2 M, pH 7.4), containing 0.25 mM $MgCl_2$. The incubation was performed in the presence and absence of an NADPH generating system: 1 mM glucose-6-phosphate (Sigma Aldrich, USA) 0.1 mM NADP+ (Sigma Aldrich, USA) and 1 unit/ml glucose-6-phosphate dehydrogenase (G6PDH-, Sigma Aldrich, USA). The reactions were incubated at 30 °C with 1250 rpm oscillation and stopped at 0, 15 min, and 2 h time points using 100 µl acetonitrile and stirred additionally for 30 min. Finally, the quenched reactions were centrifuged at 10,000 rpm for 10 min and the supernatant was transferred to HPLC vials, with 100 µl of the supernatant loaded for HPLC analysis. Reactions

were performed in triplicate and compared against a negative control with no NADPH regenerating system to calculate substrate depletion. Amitraz, DPMF and chlorfenapyr were separated on a 5 µm C18 (250 mm × 4.5 mm) reverse phase analytical column (Fortis Technologies, UK). Amitraz was separated using an isocratic mobile phase of 80% acetonitrile and 20% H_20 with a flow rate of 1.5 ml min^{-1} for 20 min. Reactions were monitored by changes in absorbance at 313 nm and quantified by peak integration (Chromeleon, Dionex). For enzyme reaction kinetics, different concentrations of amitraz were used. Rates of substrate turnover from two independent reactions were plotted versus substrate concentration. Km, Vmax and Kcat were determined using SigmaPlot (v.12.0) (Systat Sofware, UK). DPMF was separated under binary gradient conditions. The program used was initially 1.5 min with an isocratic mobile phase of acetonitrile, 0.01 M TEA, pH 6.1 (adjusted with 0.75 M H_3PO_4), 30:70 (v/v), and then a linear gradient was applied arriving at 100% acetonitrile at 20 min. The flow rate was 1 mL/min. Reactions were monitored by changes in absorbance at 210 nm and quantified by peak integration (Chromeleon, Dionex). Chlorfenapyr was separated on a 5 µm C18 (250 mm × 4.5 mm) reverse phase analytical column (Fortis Technologies, UK). Reactions with chlorfenapyr were separated using an isocratic mobile phase of 85% methanol and 15% of 40 mM ammonium acetate in water with a flow rate was 0.8 ml min^{-1} for 7 min.

2.7.2 Identification of reaction products of amitraz and chlorfenapyr by LC-MS analysis

The reactions of the P450 enzymes with amitraz and chlorfenapyr, respectively, in the presence and absence of an NADPH generating system were further analyzed using a high-resolution HPLC-MS/MS system. Sample injections of 1 µl and 10 µl volumes were performed for amitraz and chlorfenapyr, respectively, via an Ultimate 3000 Autosampler (Thermo Scientific, USA). Chromatographic separation was achieved using an Ultimate 3000 (Thermo Scientific, USA), equipped with a 3 µm C18 (100 x 2.1 mm) reverse phase analytical column (Fortis Technologies, UK). Amitraz reactions were analyzed with an isocratic mobile phase of 85% acetonitrile and 15% H_20 with a flow rate of 0.2 ml min^{-1} for 12 min. Chlorfenapyr reactions were analyzed with an isocratic mobile phase of 85% MeOH and 15% of 40 mM ammonium acetate, with a flow rate of 0.2 ml min^{-1} for 7 min. Analyte detection was achieved using an electrospray ionization (ESI) Q Exactive Hybrid Quadrupole-Orbitrap Mass Spectrometer (Thermo Scientific, USA), operated in the positive ion mode for amitraz and in the negative ion mode for chlorfenapyr. Mass spectrometry was operated both in full scan/extracted ion monitoring and parallel reaction monitoring (PRM). The system was controlled by the Xcalibur (v.4.0) software (Thermo Scientific, USA), which was also used for data acquisition and analysis. The

optimum mass spectrometer parameters were set as follows: spray voltage at 4000 V for amitraz and 3500 V for chlorfenapyr respectively, sheath gas pressure at 20 arbitrary units, auxiliary gas pressure at 25 arbitrary units, ion transfer capillary temperature at 350 °C. In the parallel reaction monitoring for amitraz, the source collision induced dissociation at 20 eV. Sheat/aux and collision gas were high purity nitrogen. The reference substrate, tralopyril, was analyzed under the same experimental conditions as chlorfenapyr.

2.8 QTL mapping with bulked segregant analysis (BSA)

2.8.1 Experimental evolution setup

A mapping population was generated by placing 37 virgin adult females of the susceptible inbred ROS-ITi strain together with a single young male of the resistant HPC strain on a detached bean leaf. The resulting F_1 population was expanded in a climatically controlled chamber for 4-5 generations to generate a large segregating bulk population. From this bulk, 10 subpopulations were established via transfer of 500 individuals per subpopulation to potted bean plants placed in a mite-proof cage (BugDorm-4F4590DH, MegaView ScienceCo., Taiwan). These subpopulations were allowed to grow for around 5 generations under greenhouse conditions (20-25 °C and 50-80% relative humidity). Next, a paired amitraz- and chlorfenapyr-selected population was established from each of these 10 control populations by transferring around 500 adult female mites to new potted bean plants, giving rise to a total of 30 experimental populations (10 untreated control + 10 amitraz-treated + 10 chlorfenapyr-treated). Bean plants were sprayed with a gradually increasing concentration of amitraz or chlorfenapyr using a hand-held spraying device (Birchmeier, Switzerland). The initial selection concentration was 50 mg L^{-1} of amitraz and 10 mg L^{-1} chlorfenapyr, which over the course of ± 25 generations increased to 1000 mg L^{-1} amitraz and 500 mg L^{-1} chlorfenapyr, respectively. Prior to DNA extractions, acaricide susceptibility were evaluated by conducting dose-response bioassays on all amitraz/chlorfenapyr-selected and control subpopulations, following the procedure detailed in Section 2.3. Selected subpopulations were kept on unsprayed plants for one generation (10 days) before the bioassays were conducted. Mortality percentages between the paired selected and control populations were analyzed using a generalized mixed model, with a binomial distribution (SPSS v.28). Selection regime and dosage were incorporated as fixed effects in the linear model, whereas population was regarded as a random effect (Wybouw et al., 2019).

2.8.2 DNA extraction, genome sequencing, mapping and variant detection

At the end of the selection experiment, after approximately 9 months (± 25 generations), 800 adult female mites were collected from each of the 30 subpopulations for genomic DNA (gDNA) extraction. gDNA was extracted following the phenol-chloroform-based protocol as described previously (Russell and Sambrook, 2001; Van Leeuwen et al., 2008). Quantity and quality of gDNA was evaluated using a Denovix DS-11 spectrophotometer (DeNovix, USA) and by running 2% agarose gel electrophoresis (30 min at 100 V), respectively. During the initial phase of the QTL mapping experiment, a sample of 800 female mites of the resistant parental strain (HPC) was collected, and genomic DNA was extracted using the method described above. The genomic DNA data of the other susceptible parental inbred strain, ROS-ITi, was obtained from research conducted by Kurlovs et al. (2022). Illumina libraries were constructed using the TruSeq DNA PCR-free sample preparation kit and sequenced using the Illumina Novaseq 6000 technology, generating paired-end reads of 150 bp with a mean insert size of 350 bp. Genomic sequence reads for all BSA populations as well as the HPC strain were deposited in the NCBI Sequence Read Archive (SRA) under BioProject (PRJNA1033831), whereas the genomic sequence reads of the ROS-ITi strain were made available by Kurlovs et al. (2022) on the NCBI SRA under BioProject PRJNA799176. The resulting reads were aligned to the three pseudochromosome assembly of the *T. urticae* genome (Wybouw et al., 2019) using the BWA-MEM algorithm (v.0.7.17-r1188) with default settings. Subsequently the alignments were processed and position-sorted using SAMtools (v.1.11) and duplicates were marked using the Picard toolkit (v.2.20.4-SNAPSHOT). Next, HaplotypeCaller was used from the GATK package (v.4.1.7.0) to perform joint variant calling across all 30 subpopulations and the parental strains, which produced a variant call format (VCF) file containing single nucleotide polymorphisms (SNPs) and indels. The GATK tools CombineGVCF and GenotypeGVF were used to combine the gVCF's of each BSA population and the parental strains into one single VCF and do the genotyping, respectively.

2.8.3 PCA, BSA and SNPeff

To inspect the variability between and within treatment group samples, a principal component analysis (PCA) was performed using the R package prcomp (v.4.2.1), as described by Snoeck et al. (2019). More specifically, this method uses a correlation matrix containing the individual SNP frequencies as an input, and only selects SNP alleles that differentiated the two parental strains from the BSA, and were present in every treatment group (amitraz-selected, chlorfenapyr-selected and control). The PCA is represented as a two-dimensional plot with PC1

and PC2, using the function autoplot in the R package ggplot2 (v.3.3.6). The BSA analysis was performed via the script "RUN_BSA1.02.py", available at https://github.com/rmclarklab/BSA, using the final gVCF as input with default settings for paired offspring data with a haplodiploid male parent and the flags *"-perm"* set to 10000 and *"-sig"* set to 0.05 (Kurlovs et al., 2019). The final gVCF file was also used as input for the R package Gviz (v.1.40.1) (Hahne and Ivanek, 2016) for visualization of genes within interesting regions below the QTL peak, based on the GFF3 annotation of the *T. urticae* three pseudochromosome assembly published by Wybouw et al (2019) (Wybouw et al., 2019).

The package SnpEff (v.5.0c) (Cingolani et al., 2012b) was used to mine the variants predicted by GATK in the regions of the three QTLs identified in both BSA assays for SNPs and small indels with 'HIGH' and 'MODERATE' effects on the coding sequence. To this end, SnpEff uses a database derived from the three pseudochromosome assembly of the *T. urticae* genome (Wybouw et al., 2019) together with the *T. urticae* coding sequence database originating from the annotation of 23 June 2016 (available on the Online Resource for Community Annotation of Eukaryotes—ORCAE) (Sterck et al., 2012). Next, the tool SnpSift (Cingolani et al., 2012a) within the SnpEff package was used to filter the SnpEff output in the region of the common upward facing peak of QTL 1 for variants present in the resistant parent (HPC), absent in the susceptible parent (ROS-ITi) and enriched in all amitraz- or chlorfenapyr-selected populations (i.e., the allelic depth of the variant allele being higher than the allelic depth of the reference allele). For the BSA selected with amitraz, two additional downward facing peaks (QTL2 and QTL3) were identified for which the SnpEff output was filtered with SnpSift for variants where the reference allele was enriched in all amitraz-selected populations as compared to the control populations (i.e., the allelic depth of the variant allele being lower than the allelic depth of the reference allele). The variants predicted by GATK were also mined for SNPs and small indels with 'HIGH' and 'MODERATE' effects on the coding sequence of the hypothesized target-site genes of amitraz; the beta-adrenergic octopamine receptor (*βOAR*, *tetur08g04980*) and the octopamine-tyramine receptor (*tetur25g01530*).

Differential expression of the genes within the peak regions between the parents ROS-ITi and HPC was studied using the methods explained in Section 2.6. Transcriptomic data of ROS-ITi was made publicly available by Kurlovs et al. (2022) on the NCBI SRA database under BioProject PRJNA801103.

2.9 RNAi experiment

In order to test the hypothesis that the cluster of HR96-LBD genes located at QTL1 are the transcriptional regulators driving the contrasting resistance phenotypes, an RNAi experiment knocking down this cluster of genes was conducted. Gene-specific primers that contain 20 bases of the T7 promoter were designed using E-RNAi and si-Fi (Horn and Boutros, 2010; Lück et al., 2019) to amplify (1) *tetur03g00690*, *tetur03g00710*, *tetur03g00730* and *tetur03g00740* from cDNA of strain HPA and (2) GFP from plasmid DNA (primer info listed in **Supplementary Table 1**). Using the Maxima First Strand cDNA synthesis kit (Thermo Fisher Scientific, USA) cDNA from HPA was obtained via reverse transcription of RNA. Amplification was performed by PCR using GoTaq G2 Flexi DNA polymerase (Promega, USA) with initial denaturation at 95 °C for 2 min, followed by 35 cycles of amplification (95 °C for 30 s, 53 °C for 30s, 72 °C for 1 min) and a final extension at 72 °C for 5 min. PCR products were purified using E.Z.N.A. Cycle Pure kit (Omega Bio-Tek, USA) of which quality and quantity was verified using a DeNovix DS-11 FX spectrophotometer (DeNovix, USA) and by running an aliquot on a 2% agarose gel. Next, 1 µg of the T7 PCR template was used for dsRNA synthesis using the TranscriptAid T7 High Yield Transcription kit (Thermo Fisher Scientific, USA) according to the manufacturer's instructions with a reaction volume of 20 µl and an incubation at 37°C overnight. After synthesis, T7 PCR template was degraded by DNase I treatment and dsRNA was purified by chloroform-phenol extraction. Concentrations were evaluated using a DeNovix® DS-11 FX spectrophotometer (DeNovix, USA) and integrity was verified by 2% agarose gel electrophoresis. Injections of dsRNA were performed as described by Dermauw et al. (Dermauw et al., 2020a). Briefly, 120 2-3 days old adult female mites of the HPA strain were immobilized and injected with a mix of all four dsRNA fragments (500 ng/µl each) under a Leica S8 APO microscope (Leica Microsystems, Germany) with a Nanoject III microinjector (Drummond Scientific, USA) with needles pulled from 3-000-203-G/X Glass Capillaries (Drummond Scientific, USA) with a P-1000 Micropipette Puller (Sutter Instruments, USA) with settings "heat: 500, pull: 60, velocity: 70, delay: 200, pressure: 500, Ramp: 490". Needles were sharpened with a BV-10 Micropipette Beveler (Sutter Instruments, USA; 15° angles). Each female was injected with 3 nl near the third pair of legs. After injection, mites were allowed to recover on detached bean leaves on wet cotton.

Four days after injection, 50-100 mites surviving the injection of dsRNA against HR96-LBD genes (treatment) or GFP (control) were collected with four biological replicates each. RNA was extracted and sequenced as described in section 2.6.1. Prior to RNAseq, the efficiency of

the RNAi knockdown of each of four HR96 genes in the mix (*tetur03g00690*, *tetur03g00710*, *tetur03g00730* and *tetur03g00740*) was assessed by RT-qPCR using three replicates with specific primer pairs for each of the respective HR96-LDB genes (**Supplementary Table 1**). Synthesis of cDNA was performed using the Maxima First Strand cDNA Synthesis Kit (Thermo Fischer Scientific, USA) with RT-qPCR reactions conducted using the GoTaq® qPCR Master Mix (Promega, USA) in a Mx3005P qPCR machine (Agilent Technologies, Belgium). Cycle conditions were 95 °C for 10 min followed by 40 cycles of 95 °C for 15 s, 55°C for 30 s, and 60 °C for 30 s, followed by a melting curve analysis step. The quality of the qPCR experiments, i.e. the absence of contamination and the specificity of the primer-pairs, was verified using no-template controls and melting curves, respectively. The program qbase+ (Biogazelle, Belgium) was used for the analysis of raw quantification cycle (Cq) values, which were all first normalized against the housekeeping genes ribosomal protein 49 (*Rp49, tetur18g03590*) and ubiquitin C (*UBQ, tetur03g06910*). Two technical replicates were used for each biological replicate, and mean relative expression values relative to the GFP-injected strain were presented with their standard deviations. Statistically significant differences between treatment groups were assessed using unpaired t-tests with Benjamini-Hochberg correction for multiple testing. Genome-wide differentially expressed genes between the treatment and control groups were determined with RNAseq and DESeq2 as described in section 2.6.4.

3 Results

3.1 Amitraz, chlorfenapyr and tralopyril resistance levels

Susceptibility levels of all strains are given in **Table 1**. The populations ROS-ITi and JW were susceptible to amitraz and chlorfenapyr. Resistance levels in the field collected strain HP reached 7.5-fold for amitraz and 8.4-fold for chlorfenapyr, confirming an earlier study (Simma et al., 2020). Further selection of the HP strain in the laboratory-selected with chlorfenapyr and amitraz, resulted in strains HPC and HPA, respectively. Chlorfenapyr selection dramatically increased RRs of chlorfenapyr from 8.4-fold in HP to >1500-fold in HPC, whereas amitraz-selection only resulted in a more moderate increase of amitraz RRs from 7.5-fold in HP to 51-fold in HPA. Remarkably, amitraz selection also resulted in mild increase of chlorfenapyr resistance (RRs 8.4-fold and 49-fold in HP and HPA respectively) but chlorfenapyr selection did not increase amitraz resistance (RRs 7.5-fold and 7-fold in HP and HPC, respectively). When comparing the chlorfenapyr resistance levels between HPC and JW to those of tralopyril, a significant decrease in RRs was observed from 1500-fold to 23-fold (**Table 1**).

3.2 Mode of inheritance of chlorfenapyr resistance

The chlorfenapyr mortality-response curves of F_1 females from reciprocal crosses HPC ♀ × LON ♂ (RS) and LON ♀ × HPC ♂ (SR) were nearly identical which indicated that the resistance trait inherits autosomal and partly dominant (**Supplementary Figure 1, Supplementary Table 2**). The chlorfenapyr mortality-response curve of F_2 females from the (LON ♀ × HPC ♂) ♀ × LON ♂ backcross (SR x S) is shown in **Supplementary Figure 1**. A χ^2 goodness-of-fit test showed that the observed mortality for SRxS was significantly different from the expected mortality for monogenic inheritance ($\chi 2 = 75.75$, df = 13, $P < 0.05$). However, in the F2 mortality curve a clear 'plateau' was visible around 55% mortality and the curve matched closely with the expected values for monogenic inheritance for most points **(Supplementary Table 2)**.

3.3 Effect of synergists PBO, DEF and DEM on toxicity

The toxicity of amitraz and chlorfenapyr to JW, HPA and HPC after pretreatment with synergists PBO, DEF or DEM is presented in **Table 2**. Amitraz toxicity was synergized 3.2-fold by PBO and 4.3-fold by DEF in the amitraz selected strain HPA, while DEM pretreatment had no effect. Similar findings were observed for the susceptible Ethiopian strain JW, but at considerably lower SRs of 1.4- and 1.2-fold for PBO and DEF, respectively. Pretreatment with PBO, DEF or DEM only slightly enhanced the toxicity of chlorfenapyr in the chlorfenapyr selected strain HPC with synergism ratios higher than 1.7-, 2.2- and 1.7-fold, respectively. Conversely, pretreatment with PBO caused a small antagonistic effect on the chlorfenapyr susceptible strain JW with SR of 0.85-fold. Pretreatment with DEM did not synergize the toxicity of chlorfenapyr in JW.

3.4 RNAseq analysis

3.4.1. Genome-wide transcriptional differences and clustering

To investigate the genome-wide expression changes associated with chlorfenapyr and amitraz resistance, a differential expression analysis was performed using a panel of strains. The susceptible Ethiopian strain JW, the field collected parental HP and the laboratory-selected amitraz- and chlorfenapyr resistant populations (HPA, HPC). The HPA and HPC were also analyzed when continuously exposed to chlorfenapyr and amitraz (HPAexp and HPCexp). The LON strain was used as a general reference. Illumina sequencing generated 31.145 million strand-specific paired-end reads per sample, of which an average of 84% mapped uniquely

against the *T. urticae* three chromosome reference assembly (**Supplementary Table 3**). RNA reads were submitted in the NCBI Sequence Read Archive under Bioproject (PRJNA1033836) and raw read count data was made available on Figshare (DOI 10.6084/m9.figshare.24499732). A PCA was performed using normalized read-counts of the 5000 most variable genes of the complete dataset (**Figure 1A**). This PCA revealed that PC1, which explains the largest fraction of the variance in the dataset (45%), separates JW from all other strains. PC2, which explains 26% of the variance in the dataset, separates all strains with Ethiopian origin from LON. The PCA in **Figure 1A** also indicates a larger genome-wide transcriptional effect of amitraz selection compared to chlorfenapyr because the samples of HPC, HPCexp and HP cluster closely together. The variance and clustering of the selected HP subpopulations was also investigated in PCA using normalized read-counts of the 5000 most variable genes of HP, HPA, HPC, HPAexp and HPCexp (**Supplementary figure 2**). From this PCA it was immediately clear that replicate 1 of HPC did not cluster with the other replicates and was an outlier which had to be removed for further analysis. The PCA excluding this replicate is presented in **Figure 1B** and shows clear separation of all sample groups. Interestingly, as PC1 accounts for 53% of the total variance in the dataset and PC2 for only 14%, the amitraz-selected populations clustered further away from the parental strain HP than the chlorfenapyr-selected populations. Although the treated and untreated populations still cluster together, to overall effect of induction by the respective chemicals is limited, compared to strains of different genetic origin.

To gain better insights into the global transcriptomic patterns, a k-means clustering analysis was performed, using z-scaled normalized read-counts of all genes that show significant differences in expression across all samples (p value < 0.001 as determined by LTR test). A total of 8769 genes was grouped into an optimum of 13 clusters as determined by the gap statistic (**Supplementary Table 4**). The clustered heatmap based on individual z-scores in **Figure 2A** and **Supplementary Figure 3** indicates 13 distinct transcriptomic patterns. GO enrichment analysis of all genes in each cluster (**Supplementary Table 5**), combined which the expression patterns of HP and its derived selected subpopulations, resulted in six clusters (**Figure 2B**) that sparked our interest.

Cluster 3 contains 529 genes showing lower expression levels in JW and HP whose expression increases after selection with both compounds. Many GO terms are significantly associated with the genes in this cluster. The term GO:0008152 for metabolic process is the most significantly enriched and contains five genes coding for UGTs. Also, many GO terms linked to oxidoreductase activity (GO:0055114, GO:0016491, GO:0016620) are enriched, containing

P450s of the CYP385, CYP387 and CYP389 family and *CYP392E10,* as well as multiple SDR genes. Interestingly, this cluster also contains seven genes coding for ABC transporters which lead to two terms linked to increased transporter activity to be significantly enriched (GO:0055085; "*transmembrane transport*" and GO:0005215; "*transporter activity*"). Cluster 5 contains 512 genes with specifically low expression levels in HPA whereas transcriptomic levels in all other groups remain comparable. In this cluster only two GO terms are significantly enriched; GO:0003676, containing a multitude of genes coding for Zinc Finger proteins involved in nucleic acid biding and GO:0004674 containing genes coding for proteins with serine/threonine kinase activity. Cluster 8 contains 737 genes with higher expression levels in HP and all selected subpopulations. However, no GO terms could be significantly linked in this cluster. Cluster 9 contains 594 that are specifically overexpressed only in the amitraz-selected subpopulation of HP. This cluster contains a multitude of genes belonging to different detoxification gene families resulting in highly significant enrichment of their respective GO terms. Terms linked to P450 activity; *"oxidation-reduction processes"* (GO:0055114), *"iron ion binding"* (GO:0005506), *"heme-binding"* (GO:0020037), *"oxidoreductase activity, acting on paired donors, with incorporation or reduction of molecular oxygen"* (GO:0016705) were enriched with most significant adjusted *p*-values in both the *"Molecular Function"* and *"Biological Processes"* categories. Hence, cluster 9 contains overall the most CYP (pseudo)genes and its majority belongs to the notorious CYP392 family; e.g. *CYP392A11 (tetur03g00970), CYP392A12 (tetur03g00830), CYP392A16 (tetur06g04520), CYP392D2 (tetur03g04990), CYP392D8 (tetur03g05070), CYP392E8 (tetur27g01020)* and many more. Other genes within this cluster linked to these GO terms are four intradiol ring-cleavage dioxygenase genes *DOGs* and *Cytochrome P450 reductase (CPR)*. This cluster contains also a large number UGT (15) and GST (4) genes which lead to an enrichment of terms linked to *"metabolic processes"* (GO:0016999, GO:0008152), *"transferase activity, transfer of hexosyl groups"* (GO:0016758) and *"cysteine-type peptidase activity"* (GO:0008234). However, also many other cysteine peptidase genes (4 C13 legumains and 16 cathepsin L) are grouped in cluster 9, adding to the high significance of *"cysteine-type endopeptidase activity"* (GO:0004197) as well as *"regulation of catalytic activity"* (GO:0050790) and "*proteolysis"* (GO:0006508). Last, also a highly significant enrichment of GO terms linked with transmembrane transporters (GO:0055085, GO:0006810, GO:0042626) and ATPase activity (GO:0042626, GO:0016887) was apparent because of the presence of 15 ABC-transporter genes. Cluster 10 contains 363 genes which show high transcriptional patterns only in the HP strain and is significantly linked with *"(r)RNA processing"* (GO:0006364, GO:0006396),

"RNA binding" (GO:0003723) and *"ribosome biogenesis"* (GO:0042254). Cluster 11 contains 512 genes and shows a similar transcriptomic pattern as cluster 9, with the exception of JW, which had a low z-score in cluster 9 but a higher z-score in cluster 11. A large fraction of the genes in this cluster code for ribosomal proteins associated with various translational and processes which is reflected in the enriched GO terms *"translation"* (GO:0006412) and *"structural constituent of ribosome"* (GO:0003735). However, also genes coding for elongation factors and chaperones like *DnaJ* involved in translation elongation and protein folding, respectively, are abundantly present in this cluster leading to enrichment of the respective GO terms (GO:0003746, GO:0006457, GO:0051082). Finally, this cluster is also enriched with genes coding for proteasome subunits linked with endopeptidase activity (GO:0004298, GO:0004175) and involved in proteolysis in cellular protein catabolic processes (GO:0051603).

3.4.2 Pairwise differential expression shows contrasting P450 expression patterns associated with amitraz and chlorfenapyr selection

First, pairwise differential expression analysis was performed comparing JW, HP, HPA, HPC, HPAexp and HPCexp with LON as a general reference strain (**Supplementary Table 6; Supplementary Table 7**). Immediately noticeable was that the number of differentially expressed genes (DEGs; $|Log_2FC| > 1$; p adj < 0.05) for JW was almost double the amount of DEGs in other comparisons to LON, which is also reflected in the distinct clustering of JW in the PCA plot (**Figure 1**) and largely deviating z-scores in many clusters (**Figure 2**). Moreover, the largest fraction of JW DEGs was downregulated, whereas for all other strains the largest fraction of DEGs was upregulated. Secondly, a differential expression analysis using only HPA, HPAexp, HPC and HPCexp versus the common parent HP was undertaken to specifically study DEGs following amitraz- or chlorfenapyr-selection of HP. Interestingly, the transcriptomes of selected populations with the same HP parental genetic background show differences in terms of the number of DEGs and the proportions of up- and downregulated genes depending on amitraz or chlorfenapyr selection. Amitraz selection results in a larger total number of DEGs of which the largest fraction (63% and 67% for HPA and HPAexp, respectively) was upregulated. In contrast, in the chlorfenapyr selected population the largest fraction of DEGs was downregulated (56% and 64% for HPC and HPCexp) (**Supplementary Table 6; Supplementary Table 7**). Next, given the overall abundancy of P450 genes in clusters associated with amitraz and chlorfenapyr selection (**Supplementary Table 8**), we studied the transcriptional changes of P450s due to amitraz or chlorfenapyr selection of the same

moderately resistant parent HP more closely. Results are shown in **Figure 3** as a heatmap of the Log_2FC of all full-length P450s differentially expressed (i.e. $|Log_2FC| > 1$ and p adj < 0.05) in at least one of the selected subpopulations. Strikingly, based on Euclidian clustering of the rows of the heatmap a cluster of four P450 genes, *CYP392A11, CYP392D2, CYP392D8* and *CYP392A12* showed extreme transcriptional differences; i.e. upregulation with $Log_2FCs > 4$ after amitraz selection and downregulation with $Log_2FCs < -2$ after chlorfenapyr selection. All four of these P450 genes were present in cluster 9 of the k-means clustering analysis together with many other genes linked to detoxification processes. Another cluster of P450 genes, *CYP392A16, CYP392D6* and *CYP392A15* also showed very high upregulation upon amitraz selection but did not change much upon chlorfenapyr selection. Last, *CYP392A1* is the only P450 upregulated after selection with each compound.

3.5 *In vitro* metabolism of amitraz and chlorfenapyr

3.5.1 Heterologous expression of *T. urticae* P450s in *E. coli*

Five potentially interesting P450s in this study, CYP392A16, CYP392A11, CYP392A1, CYP392E10, and CYP392D8, were co-expressed with the *T. urticae* cytochrome P450 reductase (CPR) in *E.coli* membranes, producing catalytically active monooxygenase complexes (Omura and Sato, 1964). All membrane preps produced showed the characteristic CO-reduced spectrum, which is indicative of an active P450 (**Supplementary Table 9**). In all cases, CPR activity against cytochrome c was confirmed, as shown in **Supplementary Table 9**.

3.5.2 CYP392A16-mediated hydroxylation of amitraz

All five P450s were evaluated for their potential to metabolize amitraz of which only CYP392A16 was able to do so. The catalytic activity of the P450 was assessed by measuring amitraz turnover in the presence and absence of NADPH and analyzing the formation of metabolites. Incubation of the CYP392A16 complex with amitraz for 15 min revealed a 55.9% NADPH dependent depletion of amitraz (eluting at 15.4 min) and the parallel formation of an unknown metabolite (M1, eluting at 2.17 min), as compared to the control reaction without NADPH (**Supplementary Figure 4A**). The ability of CYP392A16 to metabolize amitraz was further characterized by measuring substrate-depletion based reaction rates revealed Michaelis-Menten kinetics (R^2 of fitted curve = 0.98, **Supplementary Figure 4B**): Kcat = 36.5 (± 2.6 SE) pmol of depleted amitraz/min/pmol P450, Vmax = 182.4 (± 8.7 SE) pmol of depleted

amitraz/min and Km = 28.64 (± 3.97 SE) μM. CYP392A16 did not metabolize DMPF, as no substrate depletion was detected (data not shown).

HPLC-MS and MS/MS analysis of the reaction mixtures pointed towards hydroxylation of amitraz as the most likely reaction mechanism catalyzed by CYP392A16. However, neither the toxic metabolite of amitraz, DMPF (N-Methyl-N'-(2,4-xylyl) formamidine) nor the other known metabolites of amitraz (Giorgini et al., 2023; Guo et al., 2021; Schuntner and Thompson, 1978), DMF (2,4 dimethylformamide) and the DMA (2,4 dimethylaniline) could be detected. Nevertheless, the accurate mass HLPC-MS analysis confirmed the generation of hydroxyl-amitraz, as the major detectable metabolite M1 (**Figure 4A/B**). The positive ion mode mass spectrum of the amitraz metabolite M1 showed the molecular ion peak at m/z $[M+H]^+$ = 310.1910, which is 15.99 Da units higher than the corresponding peak in the spectrum of the parent compound at m/z $[M+ H]^+$ = 294.1961. Accurate mass measurements showed that the +15.99 Da corresponds to an O atom. Thus, the metabolite has been hydroxylated, with several hydroxylation sites being possible, according to the Biotransformer (v.3.0) theoretical tool **(Figure 4C)**. The fragmentation pattern from the MS/MS spectra of amitraz and its metabolite also showed a shift upwards by 15.99 Da in the corresponding M1 metabolite product ions (**Supplementary Figure 5),** which confirmed also hydroxylation as the likely mechanism of the reaction catalyzed by CYP392A16, but cannot propose a specific structure for the hydroxylated metabolite of amitraz.

3.5.3 CYP392D8-mediated activation of the pro-insecticide chlorfenapyr to its toxic N-dealkylated metabolite tralopyril

All five P450s were also tested for their potential role to metabolize or activate the pro-insecticide chlorfenapyr. Results from HPLC chromatograms in **Figure 5A** show that only CYP392D8 causes an NADPH-dependent depletion of chlorfenapyr eluting at 3.96 min and the formation of a metabolite eluting at 2.87 min. This metabolite corresponds possibly to the n-dealkylated metabolite tralopyril (the active toxophore of chlorfenapyr), as indicated by the same eluting time with standard tralopyril. For further confirmation we proceeded to LC-MS analysis. Chlorfenapyr and tralopyril were detected in negative ion mode, and not in the protonated molecular ion form, due to the loss of the N-ethoxymethyl group, when introduced in the ESI source. Thus, although chlorfenapyr and tralopyril have the same mass spectra (**Figure 5B**), they have different elution times (**Figure 5A**), so we confirmed that the formatted metabolite corresponds to tralopyril.

3.6 Genetic mapping of chlorfenapyr and amitraz resistance

3.6.1. Experimental evolution and phenotyping

The mapping study was started from a cross between a single haploidHPC male and females of the susceptible inbred strain ROS-ITi. Interestingly, HPC not only showed extremely high resistance levels for chlorfenapyr after chlorfenapyr selection (RR > 1500), but residual amitraz resistance (RR 7.0) was still present, which allowed to also select for amitraz resistance in the mapping population. After approximately 25 generations of treatment with increasing doses of chlorfenapyr or amitraz, both selected and unselected populations were phenotyped using dose-response bioassays. At a dose of 500 mg L^{-1}, both acaricide-selected populations showed significantly lower mortality rates compared to the control populations ($p < 0.001$, generalized mixed model) (**Figure 6A,B**). Interestingly, mortality rates of chlorfenapyr in the unselected samples do not show a dose-response relationship at doses between 20-2500 mg L^{-1} for chlorfenapyr, thus indicating segregation of a few major resistance alleles in the control populations, whereas for amitraz at 1000 mg L^{-1} mortality of the control populations is at 100% (**Supplementary Figure 6**).

3.6.2 Genetic mapping with bulked segregant analysis

Genomic DNA was extracted and sequenced and reads of all segregating populations and both parental strains (HPC and ROS-ITi) were aligned to the *T. urticae* reference genome (Grbić et al., 2011; Wybouw et al., 2019) resulting in a genomic VCF (gVCF) file containing 1,934,859 segregating high-quality SNPs distinguishing HPC from ROS-ITi. This gVCF was used for a principal component analysis (PCA) which showed grouping of the selected and control populations into distinct clusters (**Figure 6C**). To identify the genomic regions underlying chlorfenapyr and amitraz resistance, a bulked segregant analysis approach was used as described by Kurlovs et al. (2019). Briefly, this method used genome-wide differences in allele frequencies at high quality SNP loci between selected and control populations (**see gVCF available as Data S1 on Figshare: 10.6084/m9.figshare.24499732**). QTL significance was determined with a permutation-based approach as described by Snoeck et al. (2019). Using a false discovery rate (FDR) of 5%, a significantly overlapping major QTL peak could be identified on chromosome 1 (hereafter QTL1) for both the amitraz and chlorfenapyr BSA studies (**Figure 7A**). Interestingly, in the peak region spanning QTL1 (~20.850 Mb), nearly complete fixation of the MPC haplotype occurred in all amitraz-selected and chlorfenapyr-selected populations (**Supplementary Figure 7**). Based on the average difference in allele

frequencies between selected and unselected populations, there is a remarkable overlap of QTL1 in both BSA studies (**Figure 7A**). However, when considering the chromosomal locations of the actual peak maxima of both BSA's (~20.558 Mb for amitraz, ~21.108 Mb for chlorfenapyr), the averages are 500 kb away from each other (**Figure 7B**) and the individual replicability of the amitraz-selected population-pairs is lower. This has to be interpreted with caution, as there is a region in the peak where the differences in allele-frequencies drops down to zero, which is probably due to structural variability or misassembly in the *T. urticae* reference genome. As this makes it difficult to pinpoint the absolute maximum of the overlapping QTL peak, we further studied the broad genomic region surrounding the maxima of both BSA's (20.458 – 21.208 Mb) covering a region of 231 genes (**Supplementary Table 10**). Within the QTL1 peak we took a closer look at three interesting regions as outlined in **Figure 7C**. Regions A and C represent a 50 kb window surrounding the QTL1 peak maximum of the amitraz and chlorfenapyr BSA, respectively. Region B, on the other hand, is a region located around 20.9 Mb which contains a cluster of P450 genes and pseudogenes, similar to region C. Most of these P450s belong to the CYP392A family, like CYP392A11 (*tetur03g00970*) and CYP392A12 (*tetur03g00830*), located in region B, which have been directly linked with resistance in *T. urticae* before (Khalighi et al., 2016; Riga et al., 2015). However, there was no differential expression between the parental strains for these two P450s, nor were there mutations enriched in the selected populations. In contrast, other members of the CYP392A family located in region C, like *CYP392A15 (tetur03g09941), CYP392A13v1 (tetur08g08050)* and *CYP392A13v2 (tetur03g00020)* show high levels of differential expression (Log_2FC 4.39, 2.12 and 7.21 respectively) in the resistant parent HPC compared to the susceptible parent ROS-ITi and have several mutations enriched in the selected populations for both compounds. Apart from P450s, a carboxyl/cholinesterase (CCE20*, tetur03g00310*) and a short-chain reductase (*tetur03g00300),* coding for enzymes belonging to other important detoxification families, were located in QTL1 region. In addition to detoxification enzymes, also a cluster of four nuclear hormone receptors lacking a DNA-binding domain were found, which might play a role in *trans* regulation of detoxification (**Supplementary Table 10**), as was recently shown (Ji et al., 2023; Snoeck et al., 2019). The amitraz-selected populations showed two additional significant QTL loci on chromosome 3; QTL2 (~3.008 Mb) and QTL3 (~17.263 Mb). Strikingly, these peaks are facing downwards, which indicates that amitraz selection-pressure favors the reference haplotype. Similar to QTL1, in QTL2 also multiple genes coding for P450 enzymes of the CYP392A family were present, with *CYP392A10v2* (*tetur02g14400*) being the most centrally located in the peak. Also four members of the gustatory receptor family as well as three

members of the short chain dehydrogenase/reductase family (SDRs) were present. Noteworthy, one of the upregulated SDRs, *tetur02g14480*, located at ± 30 kb of the peak minimum, had two missense mutations of which the allele frequency (AF) of the variant allele is lower in selected populations compared to the control. The QTL3 region contains many transcriptional regulators which could be linked with amitraz resistance. Amongst these we found a Myc-type, basic helix-loop-helix (bHLH) domain (*tetur09g04370*), three Zinc fingers; C2H2-type (*tetur09g04260, tetur09g04200, tetur09g04190*), a Myb/SANT-like DNA-binding domain (*tetur09g04230*) and two eukaryotic translation initiation factors (*tetur09g92869, tetur09g04090*). Remarkably, the two previously hypothesized target-genes of amitraz; the beta-adrenergic octopamine receptor (*βOAR*, *tetur08g04980*) and the octopamine-tyramine receptor (*tetur25g01530*), did not occur in any of the QTLs, nor were any differences in SNPs in their coding sequences between selected and unselected populations.

3.7 RNAi of a cluster HR96-like genes

To test if the cluster of nuclear hormone genes only containing a ligand binding domain (HR96-LBD) in the region of QTL1 (*tetur03g00690*, *tetur03g00710*, *tetur03g00730* and *tetur03g00740)* impacts the expression levels of important detoxification genes, an RNAi experiment was performed where all four of these tandem genes were knocked-down simultaneously. As a control, RNAi injections were also performed with the sequence for GFP. The amitraz-selected strain HPA was used for injections for practical reasons as the marker P450 genes, including *CYP392A16* which has shown to be metabolically active against amitraz, are upregulated in this strain. Thus, if the cluster of HR96-LBD genes are indeed the transcriptional regulators, silencing them via RNAi would result in lower transcription levels of the P450 genes, which is more straightforward to confirm. First, RT-qPCR was done to verify the silencing efficiency of each of the four genes in the HR96-LBD cluster using gene-specific primer pairs (**Supplementary Table 1)**. As shown in **Supplementary Figure 8,** RT-qPCR results showed that expression for each of HR96-LBD genes was reduced by ~41-76% following dsRNA injection as compared to the control. However, despite the trend visible for *tetur03g00740,* difference in expression levels was not significant ($p > 0.05$). Also the expression level of *CYP392A16* was validated following silencing of the HR96-LBD cluster but no differences in expression levels were detected. Last, also RNAseq results showed very little difference between the dsRNA and control datasets with resulting in high adjusted *p* values after correction for multiple testing and only two genes surviving the statistical cutoff (p adj < 0.05); *tetur03g00710* coding for one of the silenced HR96 genes (Log_2FC -1.29) and

tetur05g04420 (Log_2FC -0.34) coding for a choline/ethanolaminephosphotransferase 1 (**Supplementary Table 11**).

4 Discussion

Although our understanding of acaricide and insecticide resistance in key pest species is steadily increasing, the mechanisms of amitraz and chlorfenapyr resistance have remained enigmatic to date, as only few studies report on incidence and molecular genetic mechanisms (Chen et al., 2007; Corley et al., 2013; De Rouck et al., 2023; Takata et al., 2020; Van Leeuwen et al., 2006). This is true despite the potential great economic importance of chlorfenapyr, that has shown promise for control of pyrethroid-resistant malaria vectors like *A. gambiae* (Ngufor et al., 2016; Tchouakui et al., 2023). Also amitraz is essential in the control of several important ectoparasites, like the southern cattle tick, *R. microplus,* which poses a constant threat to livestock tropical and sub-tropical regions all over the world (Jonsson, 2018). In addition, amitraz is one of the few selective acaricide for in-hive use and crucial for the control of *Varroa* populations in commercial beekeeping operations worldwide (Kamler et al., 2016; Rinkevich, 2020).

In a large screening study, an Ethiopian field strain of *T. urticae* (strain HP) was identified that showed first evidence of moderate resistance to both chlorfenapyr and amitraz (Simma et al., 2020), which prompted us to further investigate the underlying resistance mechanisms. In this study we subjected the HP strain to laboratory selection with chlorfenapyr resulting in the HPC strain. Toxicity assays revealed very high resistance levels (RR > 1500-fold) in HPC after only a few selection cycles of HP (RR 8.4-fold), suggesting that relevant genetic variation was sampled from the field. As chlorfenapyr is a pro-acaricide which needs *in vivo* oxidative activation to the toxic metabolite tralopyril (Black et al., 1994), also tralopyril toxicity was assessed. Toxicity bio-assays revealed a dramatic decrease in the resistance ratio for tralopyril compared to chlorfenapyr (from over 1500-fold to only 23-fold, respectively) in HPC, which hints towards reduced activation of the pro-acaricide as a potential resistance mechanism, although other pharmacokinetic mechanisms could not be excluded. Nevertheless, activation of chlorfenapyr by P450s could be inferred from synergism experiments, as toxicity was reduced in the susceptible strain JW (SR 0.85-fold) after pre-treatment with PBO, most likely due to the inhibition of P450-mediated oxidative removal of the chlorfenapyr *N*-ethoxymethyl group which results in its active metabolite, tralopyril (Black et al., 1994). This finding is consistent with studies demonstrating antagonism between PBO and chlorfenapyr in various insects and mites (Ahmed and Vogel, 2015; Ohnuki et al., 2023; Raghavendra et al., 2011a, 2011b; Ullah et al., 2016; Wang et al., 2019). However, PBO exhibited a minor synergistic effect in the resistant strain HPC rather than an antagonistic effect. One potential explanation of this

observation could be that in the resistant strain the expression of relevant activating P450s is already low. This would prohibit metabolic activation to tralopyril and mask the antagonistic effect of PBO in toxicity. In term, the limited synergistic effects observed could indicate the involvement of P450s that detoxify chlorfenapyr as a minor mechanism. Noteworthy, synergism experiments also revealed a minor synergistic effect of DEF and DEM in the resistant strain (SR 2.2 and 1.7, respectively), also implying that additional detoxification mechanisms, next to decreased activation, are potentially involved. With the intention to identify specific candidate genes linked with these hypothesis of resistance mechanisms, we conducted a comprehensive genome-wide RNAseq based transcriptomic study. Differential expression analysis between the chlorfenapyr-selected strain HPC and the parental strain HP showed that a cluster of P450s - *CYP392A11, CYP392A12, CYP392D2* and *CYP392D8* - were largely downregulated, which is a striking result as numerous studies have linked overexpression of these P450s with resistance against various acaricidal compounds (Dermauw et al., 2013; Khalighi et al., 2016; Piraneo et al., 2015; Riga et al., 2014; Xu et al., 2021). All four P450s belong to the notorious CYP392 subfamily, that underwent a spider mite-specific expansion (Dermauw et al., 2020b; Grbić et al., 2011) and of which many members have been shown to metabolize acaricides in *T. urticae* (For a review, see De Rouck et al., 2023). Downregulation associated with resistance also stood out from the genome-wide k-means clustering analysis, as cluster 9 contains a multitude of genes belonging to the important detoxification gene families of the UGTs, GSTs, P450s as well as many ABC-transporters. Of all clusters, cluster 9 also contained the most P450s belonging to the CYP392 subfamily, including *CYP392A11, CYP392A12, CYP392D2* and *CYP392D8,* which was also reflected in a highly significant enrichment of many P450-activity linked GO terms. These unprecedented transcriptomic patterns further strengthened our hypothesis that reduction in activation may be the main resistance mechanism and is likely associated with the downregulation of specific P450s. As the selection experiment has no replication, drift or a number of genes that regulate these detox genes cannot be excluded, but given their high expression in numerous other strains under investigation, this seems unlikely, and minimally, it can be concluded that they play no active detoxification role. Therefore, to validate these findings, the downregulated candidates *CYP392A11* and *CYP392D8*, were functionally expressed and tested for their ability to metabolize chlorfenapyr. Functional enzymes were obtained for both P450s, but metabolism assays followed by LC-MS showed that only CYP392D8 was capable to metabolize chlorfenapyr to a metabolite that was identified as tralopyril, hereby confirming that the downregulated CYP392D8 mediates activation rather than metabolization of chlorfenapyr.

Surprisingly, starting from the same parental origin HP, laboratory-selection with amitraz (strain HPA) also lead to high resistance, but this resulted in the high overexpression of the same cluster of P450 genes (*CYP392A11, CYP392A12, CYP392D2* and *CYP392D8*) with $Log_2FCs > 4$ for all of them. In HPA two other P450s were amongst the highest upregulated genes, *CYP392A1* and *CYP392A16,* whereas their expression levels were not influenced much by chlorfenapyr selection. This is in line with our synergist data, where synergist ratios for DEF and PBO indicated that esterases and P450 enzymes, respectively, likely play a significant role in amitraz resistance. This highly upregulated set of P450s from the CYP392 family were also tested for their ability to metabolize amitraz *in vitro.* CYP392A16 metabolized amitraz with high efficacy to a hydroxylated metabolite. Although the exact site and metabolite structure could not be resolved, we confirmed that the structure is different from DPMF, the known toxic metabolite of amitraz (Cai et al., 2023; Kita et al., 2017). This implies that CYP392A16 is able to metabolize amitraz, although further toxicological analysis of the metabolite is still required.

The strongly contrasting transcriptional response after selection on the same population with amitraz and chlorfenapyr is remarkable, especially that a similar cluster of detox genes, enriched in P450s responds in both opposite directions in comparison to the parental strain. It seems unlikely that this could be due to selection of many cis-effects, given that selection occurred in the laboratory with relatively small population size. As this suggests selection of a few trans factors, as recently shown for the multi-resistant strain MR-VP (Ji et al., 2023), the question remains how to identify potential genetic variation that leads to such patterns. Instead of performing an expression QTL (eQTL) analysis, which requires an exceptional amount of time and resources, we designed a genetic mapping study. As the chlorfenapyr resistant strain HPC displays this unusual pattern of downregulated detoxification genes, and because of the suggested unique mechanisms of decreased activation, we set up crosses with HPC rather than with the amitraz selected HPA. To construct a mapping population, crosses were performed between HPC strain and the susceptible inbred strain ROS-ITi. The resulting segregating populations were exposed to increasing concentrations of chlorfenapyr in an experimental evolutionary setup. Because the HPC strain was also moderately resistant to amitraz (to the same extent as the parental population), we decided to also select with amitraz, as the variation selected upon in HPA might still be segregating in HPC. This presented a unique opportunity to simultaneously conduct BSA experiment with both compounds, although the link with gene-expression is only directly relevant for HPC.

For both BSA experiments (chlorfenapyr and amitraz), one joint QTL peak on chromosome 1 (QTL1 at ~20.850 Mb) was found. For chlorfenapyr this single QTL corresponds with the nearly monogenic pattern of inheritance of resistance deduced from classical genetic crosses (fig). In the genomic region of QTL1, several detoxification genes are located, including P450s, CCEs, and UGTs. Members of the CYP392 family were overrepresented in this region, including *CYP392A11*, *CYP392A12*, *CYP392A13v1, CYP392A13v2, CYP392A14*, and *CYP392A15. In vitro* expression showed however that *CYP392A11* was not functionally active against neither acaricide. Apart from *CYP392A12,* none of the other P450s showed large transcriptional differences in HPA and HPC versus HP. Nevertheless, the two P450s for which functional validation suggested a role in resistance, *CYP392D8* for chlorfenapyr and *CYP392A16* for amitraz, were not present at QTL1, nor were the beta-adrenergic octopamine receptor (*βOAR*, *tetur08g04980*) and the octopamine-tyramine receptor (*tetur25g01530*), which recent studies have provided evidence that they are the main target-site of amitraz (Chen et al., 2007; Corley et al., 2013; Takata et al., 2020). Given the transcriptional patterns, and the lack of a clear candidate resistance gene, we then hypothesized that genetic variation (for examples multiple segregating alleles in HP) in transcriptional regulator could be responsible for the expression differences and resulting resistant phenotype. Indeed, in a recent study it was shown with allele-specific expression analysis, over a panel of resistant strains, that expression differences of P450s was mainly due to *trans* acting factors (Kurlovs et al., 2022). In a follow-up study, an extensive eQTL analysis identified variation in a duplicated HR96-related gene as the main cause of expression differences of a large group of detox genes, including CYP392A11, CYP392A12 and CYP392D8 (Ji et al., 2023). These genes belong to the nuclear hormone receptor family (HR96), but lack a DNA-binding domain (HR96-LBD). Excitingly, a cluster of genes of the same family NHR-LBD, *tetur03g00690*, *tetur03g00710*, *tetur03g00730* and *tetur03g00740* were also present in QTL1 of this study. To investigate the role of these genes in transcriptional regulation, we attempted to silence all four genes in an RNAi approach. Despite the fact that silencing efficiencies reached 41-76%, we could not observe a significant response in detoxification gene expression, which suggests that the HR96-LBD cluster located at QTL1 is not the causal factor evoking the unique transcriptional patterns observed in this study. Nevertheless, it is important to note that the HPA strain was used for RNAi experiments, whereas HPC was used in the BSA mapping. As we want to reveal downregulation after silencing HR96-LBD, a strain with high or normal expression levels is needed. However, albeit HPA and HPC share a common parent showing resistance against amitraz and chlorfenapyr, silencing of the HPA alleles of this cluster does not necessarily result in the same effect on gene

expression. Also, these HR96 genes that lack a DNA binding domain (DBD) are thought to act via ligand- or LBD-dependent dimerization with canonical NHRs that contain both LBDs and DBDs to impact gene expression (Reinking et al., 2005). Lastly, as we silenced all four HR96-LBD simultaneously, and if some level of functional redundancy exists, there might still be enough protein left that prevent clear effects on transcriptional influences at the time point of expression analysis. These hurdles could be elegantly circumvented in the future by making separate CRISPR/Cas9 induced knock-outs, a technique which recently has made big steps forward in *T. urticae* (Dermauw et al., 2020). Taking everything into account, given that the importance of the HR96-LBD cluster cannot be ruled out, we were not able to draw definite conclusive about candidate resistance genes in QTL1 involved in resistance.

Interestingly, in the amitraz selected lines two additional sharp downward facing QTL peaks on chromosome 3, QTL2 (~3.008 Mb) and QTL3 (~17.263 Mb), were observed. Such downward facing QTL peaks have not been seen in spider mite BSA experiments before (Bryon et al., 2017; De Beer et al., 2022b, 2022a; Demaeght et al., 2014; Snoeck et al., 2019; Sugimoto et al., 2020; Van Leeuwen et al., 2012; Wybouw et al., 2019) and indicate that depletion rather than enrichment of the variant alleles present in the HPC strain was favored upon selection with amitraz. In our setup, where the chlorfenapyr selected strain was used for BSA with amitraz selection, this potentially indicates that genetic variation selected by chlorfenapyr leads to susceptibility to amitraz and is purified over the selection period. In these QTLs again many genes belonging to important detox families like P450s, SDRs and cathepsins were present, but importantly, also many candidate genes involved in transcription regulation (e.g. a Myc-type, basic helix-loop-helix (bHLH) domain, Zinc fingers of the C2H2-type, a Myb/SANT-like DNA-binding domain, and eukaryotic translation initiation factors). The intricate interplay between these loci, leading to significant alterations in overall expression levels and resistance, remains to be elucidated and calls for further in-depth investigation.

To conclude, this study reveals that laboratory selection with amitraz and chlorfenapyr, starting from the same parental origin, leads to highly resistant strains to both compounds, but with clearly contrasting transcriptomic profiles. Functional validation of key P450s showed that the overexpressed CYP392A16 efficiently metabolizes amitraz, while the downregulated P450 CYP392D8 activates chlorfenapyr to its active metabolite tralopyril. The latter is potentially one of the rare cases of decreased activation as a likely resistance mechanism. Genetic mapping experiments revealed that resistance to chlorfenapyr and amitraz shared a single common major QTL, while two additional specific QTLs were uncovered for amitraz resistance. Although

these QTLs revealed promising transcription factor candidates, further validation is needed to dissect the role of individual genes in gene regulation.

Data availability statement

All the sequence data generated in this study have been submitted to the NCBI Sequence Read Archive (SRA) under Bioprojects PRJNA1033836 for RNA data and PRJNA1033831 for DNA data. Datasets needed to recreate the figures shown in this article have been deposited in Figshare (DOI 10.6084/m9.figshare.24499732).

References:

Abbott, W.S., 1987. A method of computing the effectiveness of an insecticide. 1925. J. Am. Mosq. Control Assoc. 3, 302–303.

Aguilar-Medel, S., Díaz-Gómez, O., Rodríguez-Maciel, J.C., González-Camacho, J.E., García-Velasco, R., Martínez-Carrillo, J.L., Reséndiz-García, B., 2011. *Tetranychus urticae* Koch resistance to acaricides in greenhouse rose production in Mexico. Southwest. Entomol. 36, 363–371. https://doi.org/10.3958/059.036.0313

Ahmed, M.A.I., Vogel, C.F.A., 2015. Synergistic action of octopamine receptor agonists on the activity of selected novel insecticides for control of dengue vector *Aedes aegypti* (Diptera: Culicidae) mosquito. Pestic. Biochem. Physiol., Mode of Action of Environmental Pollutants and Insecticides 120, 51–56. https://doi.org/10.1016/j.pestbp.2015.01.014

AI-Antary, T.M., AI-Lala, M.R.K., Abdel-Wali, M.I., 2012. Residual effect of six acaricides on the two spotted spider mite (*Tetranychus urticae* Koch) females on cucumber under plastic houses conditions in three upper lands regions in Jordan. Adv. Environ. Biol. 2992–2998.

Anders, S., Pyl, P.T., Huber, W., 2015. HTSeq--a Python framework to work with high-throughput sequencing data. Bioinformatics 31, 166–169. https://doi.org/10.1093/bioinformatics/btu638

Andrews, S., 2010. FastQC: a quality control tool for high throughput sequence data. https://www.bioinformatics.babraham.ac.uk/projects/fastqc/ (accessed 1.1.22).

Baron, S., Merwe, N.A. van der, Madder, M., Maritz-Olivier, C., 2015. SNP analysis infers that recombination is involved in the evolution of amitraz resistance in *Rhipicephalus microplus*. PLOS One 10, e0131341. https://doi.org/10.1371/journal.pone.0131341

Black, B.C., Hollingworth, R.M., Ahammadsahib, K.I., Kukel, C.D., Donovan, S., 1994. Insecticidal action and mitochondrial uncoupling activity of AC-303,630 and related halogenated pyrroles. Pestic. Biochem. Physiol. 50, 115–128. https://doi.org/10.1006/pest.1994.1064

Bryon, A., Kurlovs, A.H., Dermauw, W., Greenhalgh, R., Riga, M., Grbić, M., Tirry, L., Osakabe, M., Vontas, J., Clark, R.M., Van Leeuwen, T., 2017. Disruption of a horizontally transferred phytoene desaturase abolishes carotenoid accumulation and diapause in *Tetranychus urticae*. Proc. Natl. Acad. Sci. 114. https://doi.org/10.1073/pnas.1706865114

Cai, P., Zhang, Yuanyuan, Yang, M., Zhang, C., Li, M., Xiao, W., Xu, Z., Zhang, Yongqiang, 2023. Target identification and acaricidal activity difference of amitraz and its metabolite DPMF in *Tetranychus cinnabarinus* (Boisduval). Pest Manag. Sci. ps.7500. https://doi.org/10.1002/ps.7500

Chen, A.C., He, H., Davey, R.B., 2007. Mutations in a putative octopamine receptor gene in amitraz-resistant cattle ticks. Vet. Parasitol. 148, 379–383. https://doi.org/10.1016/j.vetpar.2007.06.026

Chevillon, C., Ducornez, S., De Meeus, T., Koffi, B.B., Huguette Gaïa, Delathière, J.-M., Barré, N., 2007. Accumulation of acaricide resistance mechanisms in *Rhipicephalus (Boophilus) microplus* (Acari: Ixodidae) populations from New Caledonia Island. Vet. Parasitol. 147, 276–288. https://doi.org/10.1016/j.vetpar.2007.05.003

Cingolani, P., Patel, V.M., Coon, M., Nguyen, T., Land, S.J., Ruden, D.M., Lu, X., 2012a. Using *Drosophila melanogaster* as a model for genotoxic chemical mutational studies with a new program, SnpSift. Front. Genet. 3. https://doi.org/10.3389/fgene.2012.00035

Cingolani, P., Platts, A., Wang, L.L., Coon, M., Nguyen, T., Wang, L., Land, S.J., Lu, X., Ruden, D.M., 2012b. A program for annotating and predicting the effects of single nucleotide polymorphisms, SnpEff. Fly (Austin) 6, 80–92. https://doi.org/10.4161/fly.19695

Corley, S.W., Jonsson, N.N., Piper, E.K., Cutullé, C., Stear, M.J., Seddon, J.M., 2013. Mutation in the *RmβAOR* gene is associated with amitraz resistance in the cattle tick *Rhipicephalus microplus*. Proc. Natl. Acad. Sci. 110, 16772–16777. https://doi.org/10.1073/pnas.1309072110

Damalas, C.A., 2009. Understanding benefits and risks of pesticide use. Sci. Res. Essays 4, 945–949.

David, M.D., 2021. The potential of pro-insecticides for resistance management. Pest Manag. Sci. 77, 3631–3636. https://doi.org/10.1002/ps.6369

David, M.-S., John, C.W., 2023. Arthropod pesticide resistance database | Michigan state universit. https://www.pesticideresistance.org/ (accessed 4.18.23).

De Beer, B., Vandenhole, M., Njiru, C., Spanoghe, P., Dermauw, W., Van Leeuwen, T., 2022a. High-resolution genetic mapping combined with transcriptome profiling reveals that both target-site resistance and increased detoxification confer resistance to the pyrethroid bifenthrin in the spider mite *Tetranychus urticae*. Biology 11, 1630. https://doi.org/10.3390/biology11111630

De Beer, B., Villacis-Perez, E., Khalighi, M., Saalwaechter, C., Vandenhole, M., Jonckheere, W., Ismaeil, I., Geibel, S., Van Leeuwen, T., Dermauw, W., 2022b. QTL mapping suggests that both cytochrome P450-mediated detoxification and target-site resistance are involved in fenbutatin oxide resistance in *Tetranychus urticae*. Insect Biochem. Mol. Biol. 145, 103757. https://doi.org/10.1016/j.ibmb.2022.103757

De Rouck, S., İnak, E., Dermauw, W., Van Leeuwen, T., 2023. A review of the molecular mechanisms of acaricide resistance in mites and ticks. Insect Biochem. Mol. Biol. 103981. https://doi.org/10.1016/j.ibmb.2023.103981

Dekeyser, M.A., 2005. Acaricide mode of action. Pest Manag. Sci. 61, 103–110. https://doi.org/10.1002/ps.994

Demaeght, P., Osborne, E.J., Odman-Naresh, J., Grbić, M., Nauen, R., Merzendorfer, H., Clark, R.M., Van Leeuwen, T., 2014. High resolution genetic mapping uncovers chitin synthase-1 as the target-site of the structurally diverse mite growth inhibitors clofentezine, hexythiazox and etoxazole in *Tetranychus urticae*. Insect Biochem. Mol. Biol. 51, 52–61. https://doi.org/10.1016/j.ibmb.2014.05.004

Dermauw, W., Jonckheere, W., Riga, M., Livadaras, I., Vontas, J., Van Leeuwen, T., 2020a. Targeted mutagenesis using CRISPR-Cas9 in the chelicerate herbivore *Tetranychus urticae*. Insect Biochem. Mol. Biol. 120, 103347. https://doi.org/10.1016/j.ibmb.2020.103347

Dermauw, W., Van Leeuwen, T., Feyereisen, R., 2020b. Diversity and evolution of the P450 family in arthropods. Insect Biochem. Mol. Biol. 127, 103490. https://doi.org/10.1016/j.ibmb.2020.103490

Dermauw, W., Wybouw, N., Rombauts, S., Menten, B., Vontas, J., Grbić, M., Clark, R.M., Feyereisen, R., Van Leeuwen, T., 2013. A link between host plant adaptation and pesticide resistance in the polyphagous spider mite *Tetranychus urticae*. Proc. Natl. Acad. Sci. 110. https://doi.org/10.1073/pnas.1213214110

Dobin, A., Davis, C.A., Schlesinger, F., Drenkow, J., Zaleski, C., Jha, S., Batut, P., Chaisson, M., Gingeras, T.R., 2013. STAR: ultrafast universal RNA-seq aligner. Bioinformatics 29, 15–21. https://doi.org/10.1093/bioinformatics/bts635

Duarte, A., Pym, A., Garrood, W.T., Troczka, B.J., Zimmer, C.T., Davies, T.G.E., Nauen, R., O'Reilly, A.O., Bass, C., 2022. P450 gene duplication and divergence led to the evolution of dual novel functions and insecticide cross-resistance in the brown planthopper *Nilaparvata lugens*. PLOS Genet. 18, e1010279. https://doi.org/10.1371/journal.pgen.1010279

Ducornez, S., Barré, N., Miller, R.J., Garine-Wichatitsky, M. de, 2005. Diagnosis of amitraz resistance in *Boophilus microplus* in New Caledonia with the modified Larval Packet Test. Vet. Parasitol. 130, 285–292. https://doi.org/10.1016/j.vetpar.2005.04.018

Feyereisen, R., Dermauw, W., Van Leeuwen, T., 2015. Genotype to phenotype, the molecular and physiological dimensions of resistance in arthropods. Pestic. Biochem. Physiol., 121, 61–77. https://doi.org/10.1016/j.pestbp.2015.01.004

Georghiou, G.P., 1969. Genetics of resistance to insecticides in houseflies and mosquitoes. Exp. Parasitol. 26, 224–255. https://doi.org/10.1016/0014-4894(69)90116-7

Giorgini, M., Taroncher, M., Tolosa, J., Ruiz, M.-J., Rodríguez-Carrasco, Y., 2023. Amitraz and Its Metabolites: Oxidative Stress-Mediated Cytotoxicity in HepG2 Cells and Study of Their Stability and Characterization in Honey. Antioxidants 12, 885. https://doi.org/10.3390/antiox12040885

Grbić, M., Van Leeuwen, T., Clark, R.M., Rombauts, S., Rouzé, P., Grbić, V., Osborne, E.J., Dermauw, W., Thi Ngoc, P.C., Ortego, F., Hernández-Crespo, P., Diaz, I., Martinez, M., Navajas, M., Sucena, É., Magalhães, S., Nagy, L., Pace, R.M., Djuranović, S., Smagghe, G., Iga, M., Christiaens, O., Veenstra, J.A., Ewer, J., Villalobos, R.M., Hutter, J.L., Hudson, S.D., Velez, M., Yi, S.V., Zeng, J., Pires-daSilva, A., Roch, F., Cazaux, M., Navarro, M., Zhurov, V., Acevedo, G., Bjelica, A., Fawcett, J.A., Bonnet, E., Martens, C., Baele, G., Wissler, L., Sanchez-Rodriguez, A., Tirry, L., Blais, C., Demeestere, K., Henz, S.R., Gregory, T.R., Mathieu, J., Verdon, L., Farinelli, L., Schmutz, J., Lindquist, E., Feyereisen, R., Van de Peer, Y., 2011. The genome of *Tetranychus urticae* reveals herbivorous pest adaptations. Nature 479, 487–492. https://doi.org/10.1038/nature10640

Guo, L., Fan, X., Qiao, X., Montell, C., Huang, J., 2021. An octopamine receptor confers selective toxicity of amitraz on honeybees and *Varroa mites*. eLife 10, e68268. https://doi.org/10.7554/eLife.68268

Hahne, F., Ivanek, R., 2016. Visualizing genomic data using Gviz and bioconductor, in: Mathé, E., Davis, S. (Eds.), Statistical Genomics: Methods and Protocols, Methods in Molecular Biology. Springer, New York, NY, pp. 335–351. https://doi.org/10.1007/978-1-4939-3578-9_16

Herron, G.A., Rophail, J., 2003. First detection of chlorfenapyr (Secure®) resistance in two-spotted spider mite (Acari: Tetranychidae) from nectarines in an Australian orchard. Exp. Appl. Acarol. 31, 131–134. https://doi.org/10.1023/B:APPA.0000005112.65573.be

Hollingworth, R.M., 1976. Chemistry, biological activity, and uses of formamidine pesticides. Environ. Health Perspect. 14, 57–69. https://doi.org/10.1289/ehp.761457

Horn, T., Boutros, M., 2010. E-RNAi: a web application for the multi-species design of RNAi reagents—2010 update. Nucleic Acids Res. 38, W332–W339. https://doi.org/10.1093/nar/gkq317

Ji, M., Vandenhole, M., De Beer, B., De Rouck, S., Villacis-Perez, E., Feyereisen, R., Clark, R.M., Van Leeuwen, T., 2023. A nuclear receptor HR96-related gene underlies large trans-driven differences in detoxification gene expression in a generalist herbivore. Nat. Commun. 14, 4990. https://doi.org/10.1038/s41467-023-40778-w

Jonsson, N.N., 2018. Molecular biology of amitraz resistance in cattle ticks of the genus *Rhipicephalus* . Front. Biosci. 23, 796–810. https://doi.org/10.2741/4617

Khajehali, J., Van Nieuwenhuyse, P., Demaeght, P., Tirry, L., Van Leeuwen, T., 2011. Acaricide resistance and resistance mechanisms in *Tetranychus urticae* populations from rose greenhouses in the Netherlands. Pest Manag. Sci. 67, 1424–1433. https://doi.org/10.1002/ps.2191

Khalighi, M., Dermauw, W., Wybouw, N., Bajda, S., Osakabe, M., Tirry, L., Van Leeuwen, T., 2016. Molecular analysis of cyenopyrafen resistance in the two-spotted spider mite *Tetranychus urticae*. Pest Manag. Sci. 72, 103–112. https://doi.org/10.1002/ps.4071

Kita, T., Hayashi, T., Ohtani, T., Takao, H., Takasu, H., Liu, G., Ohta, H., Ozoe, F., Ozoe, Y., 2017. Amitraz and its metabolite differentially activate α - and β -adrenergic-like octopamine receptors: Amitraz actions on octopamine receptors. Pest Manag. Sci. 73, 984–990. https://doi.org/10.1002/ps.4412

Kojima, K., Schaffer, H.E., 1967. Survival process of linked mutant genes. Evolution 21, 518–531. https://doi.org/10.2307/2406613

Kurlovs, A.H., Beer, B.D., Ji, M., Vandenhole, M., Meyer, T.D., Feyereisen, R., Clark, R.M., Leeuwen, T.V., 2022. *Trans*-driven variation in expression is common among detoxification genes in the extreme generalist herbivore *Tetranychus urticae*. PLOS Genet. 18, e1010333. https://doi.org/10.1371/journal.pgen.1010333

Kurlovs, A.H., Snoeck, S., Kosterlitz, O., Van Leeuwen, T., Clark, R.M., 2019. Trait mapping in diverse arthropods by bulked segregant analysis. Curr. Opin. Insect Sci. 36, 57–65. https://doi.org/10.1016/j.cois.2019.08.004

Leonard, P.K., 2000. Chlorfenapyr, a novel IPM compatible resistance management tool for fruit production. Acta Hortic. 257–276. https://doi.org/10.17660/ActaHortic.2000.525.30

Li, H., Handsaker, B., Wysoker, A., Fennell, T., Ruan, J., Homer, N., Marth, G., Abecasis, G., Durbin, R., 1000 Genome Project Data Processing Subgroup, 2009. The sequence alignment/map format and SAMtools. Bioinformatics 25, 2078–2079. https://doi.org/10.1093/bioinformatics/btp352

Li, R., Wang, K., Xia, X., 2005. Resistance selection by meilingmycin and chlorfenapyr and activity changes of detoxicated enzymes in *Tetranychus urticae*. Acta Phytophylacica Sin. 32, 309–313.

Love, M.I., Huber, W., Anders, S., 2014. Moderated estimation of fold change and dispersion for RNA-seq data with DESeq2. Genome Biol. 15, 550. https://doi.org/10.1186/s13059-014-0550-8

Lovell, J., Wright Jr, D., Gard, I., Miller, T., Treacy, M., Addor, R., Kamhi, V., 1990. AC 303,630-An insecticide/acaricide from a novel class of chemistry. Presented at the Brighton Crop Protection Conference, Pests and Diseases-1990. Vol. 1., British Crop Protection Council, pp. 43–48.

Lück, S., Kreszies, T., Strickert, M., Schweizer, P., Kuhlmann, M., Douchkov, D., 2019. siRNA-finder (si-Fi) software for RNAi-target design and off-target prediction. Front. Plant Sci. 10, 1023. https://doi.org/10.3389/fpls.2019.01023

Migeon, A., Nouguier, E., Dorkeld, F., 2010. Spider mites web: a comprehensive database for the Tetranychidae, in: Sabelis, M.W., Bruin, J. (Eds.), Trends in Acarology. Springer Netherlands, Dordrecht, pp. 557–560. https://doi.org/10.1007/978-90-481-9837-5_96

Ngufor, C., Critchley, J., Fagbohoun, J., N'Guessan, R., Todjinou, D., Rowland, M., 2016. Chlorfenapyr (A Pyrrole Insecticide) Applied Alone or as a Mixture with Alpha-Cypermethrin for Indoor Residual Spraying against Pyrethroid Resistant Anopheles gambiae sl: An Experimental Hut Study in Cove, Benin. PLOS ONE 11, e0162210. https://doi.org/10.1371/journal.pone.0162210

Nicastro, R.L., Sato, M.E., Arthur, V., da Silva, M.Z., 2013. Chlorfenapyr resistance in the spider mite *Tetranychus urticae*: stability, cross-resistance and monitoring of resistance. Phytoparasitica 41, 503–513. https://doi.org/10.1007/s12600-013-0309-x

Ohnuki, S., Osawa, Y., Matsumoto, T., Tokishita, S., Fujiwara, S., 2023. Utilization of piperonyl butoxide and 1-aminobenzotriazole for metabolic studies of toxic chemicals in *Daphnia magna* and *Chironomus yoshimatsui*. Ecotoxicology 32, 25–37. https://doi.org/10.1007/s10646-022-02617-4

Omura, T., Sato, R., 1964. The carbon monoxide-binding pigment of liver microsomes: I evidence for its hemoprotein nature. J. Biol. Chem. 239, 2370–2378.

Pimprale, S.S., Besco, C.L., Bryson, P.K., Brown, T.M., 1997. Increased susceptibility of pyrethroid-resistant tobacco budworm (Lepidoptera: Noctuidae) to chlorfenapyr. J. Econ. Entomol. 90, 49–54.

Piraneo, T.G., Bull, J., Morales, M.A., Lavine, L.C., Walsh, D.B., Zhu, F., 2015. Molecular mechanisms of *Tetranychus urticae* chemical adaptation in hop fields. Sci. Rep. 5, 17090. https://doi.org/10.1038/srep17090

Raghavendra, K., Barik, T.K., Bhatt, R.M., Srivastava, H.C., Sreehari, U., Dash, A.P., 2011a. Evaluation of the pyrrole insecticide chlorfenapyr for the control of *Culex quinquefasciatus* Say. Acta Trop. 118, 50–55. https://doi.org/10.1016/j.actatropica.2011.02.001

Raghavendra, K., Barik, T.K., Sharma, P., Bhatt, R.M., Srivastava, H.C., Sreehari, U., Dash, A.P., 2011b. Chlorfenapyr: a new insecticide with novel mode of action can control pyrethroid resistant malaria vectors. Malar. J. 10, 16. https://doi.org/10.1186/1475-2875-10-16

Reinking, J., Lam, M.M.S., Pardee, K., Sampson, H.M., Liu, S., Yang, P., Williams, S., White, W., Lajoie, G., Edwards, A., Krause, H.M., 2005. The Drosophila Nuclear Receptor E75 Contains Heme and Is Gas Responsive. Cell 122, 195–207. https://doi.org/10.1016/j.cell.2005.07.005

Riga, M., Bajda, S., Themistokleous, C., Papadaki, S., Palzewicz, M., Dermauw, W., Vontas, J., Leeuwen, T.V., 2017. The relative contribution of target-site mutations in complex acaricide resistant phenotypes as assessed by marker assisted backcrossing in *Tetranychus urticae*. Sci. Rep. 7, 9202. https://doi.org/10.1038/s41598-017-09054-y

Riga, M., Myridakis, A., Tsakireli, D., Morou, E., Stephanou, E.G., Nauen, R., Van Leeuwen, T., Douris, V., Vontas, J., 2015. Functional characterization of the *Tetranychus urticae CYP392A11*, a cytochrome P450 that hydroxylates the METI acaricides cyenopyrafen and fenpyroximate. Insect Biochem. Mol. Biol. 65, 91–99. https://doi.org/10.1016/j.ibmb.2015.09.004

Riga, M., Tsakireli, D., Ilias, A., Morou, E., Myridakis, A., Stephanou, E.G., Nauen, R., Dermauw, W., Van Leeuwen, T., Paine, M., Vontas, J., 2014. Abamectin is metabolized by CYP392A16, a cytochrome P450 associated with high levels of acaricide resistance

in *Tetranychus urticae*. Insect Biochem. Mol. Biol. 46, 43–53. https://doi.org/10.1016/j.ibmb.2014.01.006
Russell, D.W., Sambrook, J., 2001. Molecular cloning: a laboratory manual. Cold Spring Harbor Laboratory Cold Spring Harbor, NY.
Schuntner, C.A., Thompson, P.G., 1978. Metabolism of [14C]amitraz in larvae of *Boophilus microplus*. Aust. J. Biol. Sci. 31, 141–148. https://doi.org/10.1071/bi9780141
Sheppard, C.D., Joyce, J.A., 1998. Increased susceptibility of pyrethroid-resistant horn flies (Diptera: Muscidae) to chlorfenapyr. J. Econ. Entomol. 91, 398–400.
Simma, E.A., Hailu, B., Jonckheere, W., Rogiers, C., Duchateau, L., Dermauw, W., Van Leeuwen, T., 2020. Acaricide resistance status and identification of resistance mutations in populations of the two-spotted spider mite *Tetranychus urticae* from Ethiopia. Exp. Appl. Acarol. 82, 475–491. https://doi.org/10.1007/s10493-020-00567-2
Smith, J.M., Haigh, J., 1974. The hitch-hiking effect of a favourable gene. Genet. Res. 23, 23–35. https://doi.org/10.1017/S0016672300014634
Snoeck, S., Greenhalgh, R., Tirry, L., Clark, R.M., Van Leeuwen, T., Dermauw, W., 2017. The effect of insecticide synergist treatment on genome-wide gene expression in a polyphagous pest. Sci. Rep. 7, 13440. https://doi.org/10.1038/s41598-017-13397-x
Snoeck, S., Kurlovs, A.H., Bajda, S., Feyereisen, R., Greenhalgh, R., Villacis-Perez, E., Kosterlitz, O., Dermauw, W., Clark, R.M., Van Leeuwen, T., 2019. High-resolution QTL mapping in *Tetranychus urticae* reveals acaricide-specific responses and common target-site resistance after selection by different METI-I acaricides. Insect Biochem. Mol. Biol. 110, 19–33. https://doi.org/10.1016/j.ibmb.2019.04.011
Sparks, T.C., 2013. Insecticide discovery: an evaluation and analysis. Pestic. Biochem. Physiol. 107, 8–17. https://doi.org/10.1016/j.pestbp.2013.05.012
Sparks, T.C., Nauen, R., 2015. IRAC: mode of action classification and insecticide resistance management. Pestic. Biochem. Physiol., Insecticide and Acaricide Modes of Action and their Role in Resistance and its Management 121, 122–128. https://doi.org/10.1016/j.pestbp.2014.11.014
Sparks, T.C., Storer, N., Porter, A., Slater, R., Nauen, R., 2021. Insecticide resistance management and industry: the origins and evolution of the Insecticide Resistance Action Committee (IRAC) and the mode of action classification scheme. Pest Manag. Sci. 77, 2609–2619. https://doi.org/10.1002/ps.6254
Sterck, L., Billiau, K., Abeel, T., Rouzé, P., Van de Peer, Y., 2012. ORCAE: online resource for community annotation of eukaryotes. Nat. Methods 9, 1041–1041. https://doi.org/10.1038/nmeth.2242
Stone, B.F., 1968. A formula for determining degree of dominance in cases of monofactorial inheritance of resistance to chemicals. Bull. World Health Organ. 38, 325–326.
Sugimoto, N., Takahashi, A., Ihara, R., Itoh, Y., Jouraku, A., Van Leeuwen, T., Osakabe, M., 2020. QTL mapping using microsatellite linkage reveals target-site mutations associated with high levels of resistance against three mitochondrial complex II inhibitors in *Tetranychus urticae*. Insect Biochem. Mol. Biol. 123, 103410. https://doi.org/10.1016/j.ibmb.2020.103410
Takata, M., Misato, S., Ozoe, F., Ozoe, Y., 2020. A point mutation in the β-adrenergic-like octopamine receptor: possible association with amitraz resistance. Pest Manag. Sci. 76, 3720–3728. https://doi.org/10.1002/ps.5921
Tchouakui, M., Assatse, T., Tazokong, H.R., Oruni, A., Menze, B.D., Nguiffo-Nguete, D., Mugenzi, L.M.J., Kayondo, J., Watsenga, F., Mzilahowa, T., Osae, M., Wondji, C.S., 2023. Detection of a reduced susceptibility to chlorfenapyr in the malaria vector *Anopheles gambiae* contrasts with full susceptibility in *Anopheles funestus* across Africa. Sci. Rep. 13, 2363. https://doi.org/10.1038/s41598-023-29605-w

Terada, H., 1990. Uncouplers of oxidative phosphorylation. Environ. Health Perspect. 87, 213–218. https://doi.org/10.1289/ehp.9087213

Tibshirani, R., Walther, G., Hastie, T., 2001. Estimating the number of clusters in a data set via the gap statistic. J. R. Stat. Soc. Ser. B Stat. Methodol. 63, 411–423. https://doi.org/10.1111/1467-9868.00293

Ullah, S., Shah, R.M., Shad, S.A., 2016. Genetics, realized heritability and possible mechanism of chlorfenapyr resistance in *Oxycarenus hyalinipennis* (Lygaeidae: Hemiptera). Pestic. Biochem. Physiol. 133, 91–96. https://doi.org/10.1016/j.pestbp.2016.02.007

Van Laecke, K., Degheele, D., 1993. Effect of insecticide—synergist combinations on the survival of *Spodoptera exigua*. Pestic. Sci. 37, 283–288. https://doi.org/10.1002/ps.2780370308

Van Leeuwen, T., Demaeght, P., Osborne, E.J., Dermauw, W., Gohlke, S., Nauen, R., Grbić, M., Tirry, L., Merzendorfer, H., Clark, R.M., 2012. Population bulk segregant mapping uncovers resistance mutations and the mode of action of a chitin synthesis inhibitor in arthropods. Proc. Natl. Acad. Sci. 109, 4407–4412. https://doi.org/10.1073/pnas.1200068109

Van Leeuwen, T., Dermauw, W., 2016. The molecular evolution of xenobiotic metabolism and resistance in chelicerate mites. Annu. Rev. Entomol. 61, 475–498. https://doi.org/10.1146/annurev-ento-010715-023907

Van Leeuwen, T., Stillatus, V., Tirry, L., 2004. Genetic analysis and cross-resistance spectrum of a laboratory-selected chlorfenapyr resistant strain of two-spotted spider mite (Acari: Tetranychidae). Exp. Appl. Acarol. 32, 249–261. https://doi.org/10.1023/B:APPA.0000023240.01937.6d

Van Leeuwen, T., Tirry, L., Yamamoto, A., Nauen, R., Dermauw, W., 2015. The economic importance of acaricides in the control of phytophagous mites and an update on recent acaricide mode of action research. Pestic. Biochem. Physiol., 121, 12–21. https://doi.org/10.1016/j.pestbp.2014.12.009

Van Leeuwen, T., Van Pottelberge, S., Tirry, L., 2006. Biochemical analysis of a chlorfenapyr-selected resistant strain of *Tetranychus urticae* Koch. Pest Manag. Sci. 62, 425–433. https://doi.org/10.1002/ps.1183

Van Leeuwen, T., Van Pottelberge, S., Tirry, L., 2005. Comparative acaricide susceptibility and detoxifying enzyme activities in field-collected resistant and susceptible strains of *Tetranychus urticae*. Pest Manag. Sci. 61, 499–507. https://doi.org/10.1002/ps.1001

Van Leeuwen, T., Vanholme, B., Van Pottelberge, S., Van Nieuwenhuyse, P., Nauen, R., Tirry, L., Denholm, I., 2008. Mitochondrial heteroplasmy and the evolution of insecticide resistance: non-Mendelian inheritance in action. Proc. Natl. Acad. Sci. 105, 5980–5985. https://doi.org/10.1073/pnas.0802224105

Van Leeuwen, T., Vontas, J., Tsagkarakou, A., Dermauw, W., Tirry, L., 2010. Acaricide resistance mechanisms in the two-spotted spider mite *Tetranychus urticae* and other important Acari: a review. Insect Biochem. Mol. Biol. 40, 563–572. https://doi.org/10.1016/j.ibmb.2010.05.008

Van Pottelberge, S., Van Leeuwen, T., Khajehali, J., Tirry, L., 2009. Genetic and biochemical analysis of a laboratory-selected spirodiclofen-resistant strain of *Tetranychus urticae* Koch (Acari: Tetranychidae). Pest Manag. Sci. 65, 358–366. https://doi.org/10.1002/ps.1698

Van Pottelberge, S., Van Leeuwen, T., Van Amermaet, K., Tirry, L., 2008. Induction of cytochrome P450 monooxygenase activity in the two-spotted spider mite *Tetranychus urticae* and its influence on acaricide toxicity. Pestic. Biochem. Physiol. 91, 128–133. https://doi.org/10.1016/j.pestbp.2008.03.005

Vlogiannitis, S., Mavridis, K., Dermauw, W., Snoeck, S., Katsavou, E., Morou, E., Harizanis, P., Swevers, L., Hemingway, J., Feyereisen, R., Van Leeuwen, T., Vontas, J., 2021. Reduced proinsecticide activation by cytochrome P450 confers coumaphos resistance in the major bee parasite *Varroa destructor*. Proc. Natl. Acad. Sci. 118, e2020380118. https://doi.org/10.1073/pnas.2020380118

Wang, X., Wang, J., Cao, X., Wang, F., Yang, Y., Wu, S., Wu, Y., 2019. Long-term monitoring and characterization of resistance to chlorfenapyr in *Plutella xylostella* (Lepidoptera: Plutellidae) from China. Pest Manag. Sci. 75, 591–597. https://doi.org/10.1002/ps.5222

Wybouw, N., Kosterlitz, O., Kurlovs, A.H., Bajda, S., Greenhalgh, R., Snoeck, S., Bui, H., Bryon, A., Dermauw, W., Van Leeuwen, T., Clark, R.M., 2019. Long-term population studies uncover the genome structure and genetic basis of xenobiotic and host plant adaptation in the herbivore *Tetranychus urticae*. Genetics 211, 1409–1427. https://doi.org/10.1534/genetics.118.301803

Xu, D., Zhang, Yan, Zhang, Youjun, Wu, Q., Guo, Z., Xie, W., Zhou, X., Wang, S., 2021. Transcriptome profiling and functional analysis suggest that the constitutive overexpression of four cytochrome P450s confers resistance to abamectin in *Tetranychus urticae* from China. Pest Manag. Sci. 77, 1204–1213. https://doi.org/10.1002/ps.6130

Acknowledgements

This work was supported by the Research Council (ERC) under the European Union's Horizon 2020 research and innovation program (Grant agreement No. 772026-POLYADAPT and 773902-SuperPests) to TVL and the Special Research Fund of Ghent University (grant BOFSTA2017003701) to TVL and the Research Foundation Flanders (grant G035420N) to TVL. XL and WX were the recipients of a doctoral grant from China Scholarship Council (CSC).

Author contributions

Marilou Vandenhole: Software, Formal analysis, Investigation, Writing (Original Draft), Data Curation, Visualization, **Xueping Lu**: Formal analysis, Investigation, Writing (Original Draft), Visualization, **Dimitra Tsakireli**: Formal analysis, Investigation, Writing (Original Draft), Visualization, **Catherine Mermans**: Formal Analysis, **Sander De Rouck**: Formal Analysis, **Berdien De Beer**: Formal Analysis, **Eba Simma**: Resources, **Spiros A. Pergantis**: Supervision, formal analysis, Methodology, **Wim Jonckheere**: Writing (Review & Editing), **John Vontas**: Supervision, Funding Acquisition, **Thomas Van Leeuwen**: Conceptualization, Methodology, Funding Acquisition, Supervision, Writing (Review & Editing).

Competing interests

The authors declare no competing interests.

Main Text Tables

Table 1. LC_{50}s of amitraz, chlorfenapyr and its active metabolite tralopyril.

strain	amitraz		chlorfenapyr		tralopyril	
	LC_{50} (95% CI) (mg L^{-1})	RR[a] (95%CI)	LC_{50} (95% CI) (mg L^{-1})	RR[a] (95%CI)	LC50 (95% CI) (mg L^{-1})	RR[b] (95%CI)
LON	24 (16 - 30)	1.0	6.8 (6.1 - 7.3)	1.0	-	-
ROS-ITi	36 (30 - 42)	1.5 (1.3 - 1.8)	8.2 (7.7 - 9.1)	1.2 (1.1 - 1.3)	-	-
JW	20 (12 - 30)	0.88 (0.5 -1.3)	8.9 (8.3 - 9.2)	1.3 (1.3 - 1.4)	32 (29 - 37)	1.0
HP	180 (140 - 210)	7.5 (6.2 - 9.0)	57 (43 - 73)	8.4 (6.4 - 11)	-	-
HPA	1200 (1100 - 1300)	51 (45 - 57)	330 (270 - 410)	49 (40 - 62)	-	-
HPC	170 (140 - 190)	7.0 (6.0 - 8.1)	>10000	>1500	740 (700 - 780)	23 (21 - 25)

[a]**Resistance ratio and corresponding 95% are calculated relative to London**

[b]**Resistance ratio and corresponding 95% are calculated relative to Jimma wild**

Table 2. LC_{50}s of amitraz and chlorfenapyr with and without pre-exposure to the synergists PBO (1000 mg L^{-1}), DEM (2000 mg L^{-1}) or DEM (300 mg L^{-1} for JW and 500 mg L^{-1} for HPC and HPA).

strain	synergism	amitraz		chlorfenapyr	
		LC_{50} (95% CI) (mg L^{-1})	SR[a] (95%CI)	LC_{50} (95% CI) (mg L^{-1})	SR[a] (95%CI)
JW	**-**	20	1.0	9.0 (9.0 - 9.1)	1.0
	PBO	15 (13 - 17)	1.4 (1.2 - 1.5)	11 (10 - 11)	0.85 (0.83 - 0.87)
	DEF	17 (15 - 19)	1.2 (1.1 - 1.3)	2.7 (1.9 - 3.4)	3.4 (2.9 - 3.8)
	DEM	20 (17 - 23)	1.0 (0.9 - 1.2)	9.0 (8.8 - 9.2)	1.0 (1.0 - 1.0)
HPA	**-**	1200	1.0		
	PBO	380 (330 - 430)	3.2 (2.8 - 3.7)		
	DEF	280 (240 - 320)	4.3 (3.4 - 5.0)		
	DEM	1100 (920 - 1200)	1.1 (1.0 - 1.3)		
HPC	**-**			> 10000	1.0
	PBO			6000 (4200 - 9800)	> 1.7
	DEF			4500 (3900 - 5100)	> 2.2
	DEM			5800 (4800 - 7500)	> 1.7

[a]**Synergism ratio= LC_{50} / LC_{50} + synergist**

Main text figures

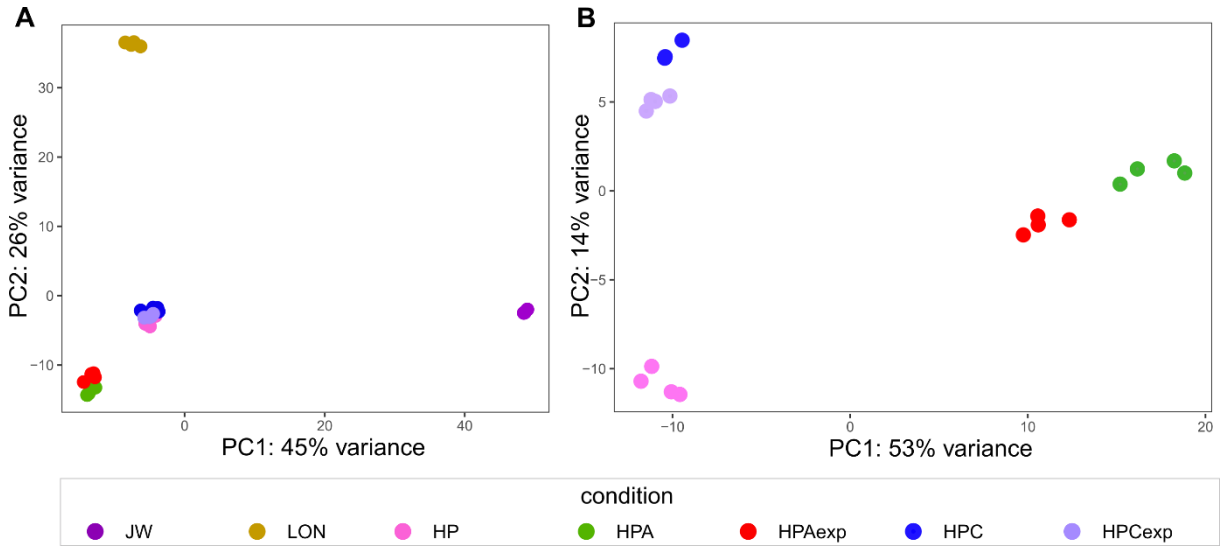

Figure 1. Principal component analysis (PCA) based on gene expression profiles of amitraz and/or chlorfenapyr resistant and susceptible strains. A) PCA based on transcriptional differences within and between all treatment groups (LON, JW, HP, HPA, HPAexp, HPC and HPCexp). B) PCA based on transcriptional differences solely due to selection pressure within and between HP and the derived laboratory-selected amitraz- or chlorfenapyr resistant subpopulations (HPA/HPAexp and HPC/HPCexp, respectively) where HPAexp and HPCexp were kept under continuous amitraz or chlorfenapyr selection pressure. PC1 and PC2 are presented on the x- and y-axis respectively, with the percentage of variance explained by each PC shown in parenthesis. The outlier HPC replicate 1 was excluded from this and all further transcriptomic analysis.

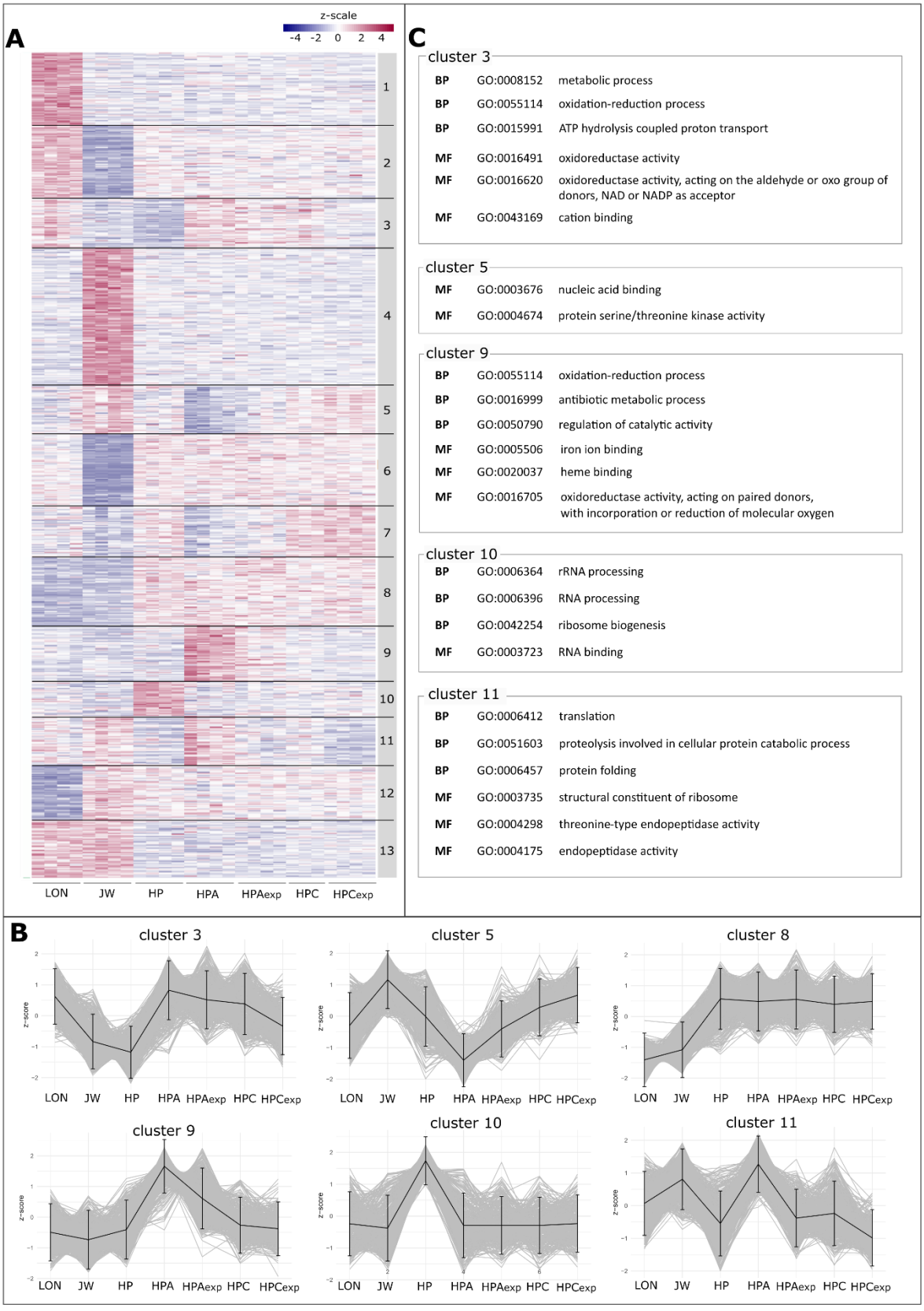

Figure 2. K-means clustering of genes based on genome wide transcriptomic differences between *T. urticae* strains LON, JW, HP, HPA, HPAexp, HPC and HPCexp. A) Genome-

wide heatmap of z-scores calculated from normalized read counts. Rows represent the genes that are grouped according to their respective clusters. B) the six most interesting clusters, plots were made representing the average z-score for all replicates per treatment group per gene in the cluster (grey lines), which was thereafter used to calculate the average z-score trend (black line) with standard deviation across all genes in the cluster. C) For the six clusters of panel B the enriched GO terms for Biological Processes (BP) and Molecular Functions (MF) are shown. Only the three most significant terms for each category are shown in case there were more.

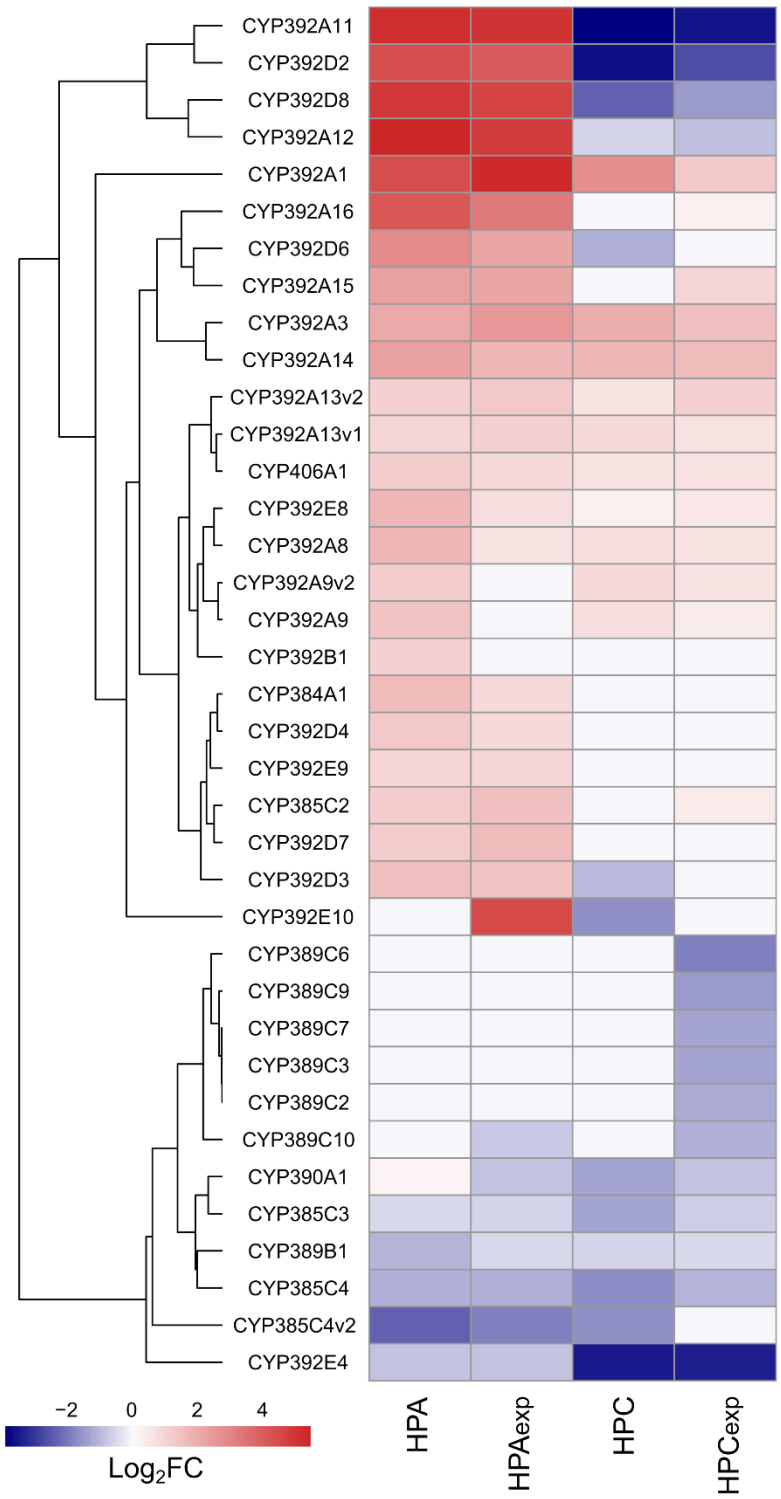

1358

1359 **Figure 3. Expression heatmap of a selection of *T. urticae* P450s.** Expression heatmap of
1360 differentially expressed full-length P450s in *T. urticae* females selected with amitraz (HPA) or

chlorfenapyr (HPC) ("exp" with continuous exposure). The Log_2 Fold Changes are relative to the expression levels in the HP strain. P450s were clustered using the Euclidian distance, and P450s that were not differentially expressed ($|Log_2FC| < 1$ and/or p value > 0.05) in all four comparisons were excluded from the heatmap.

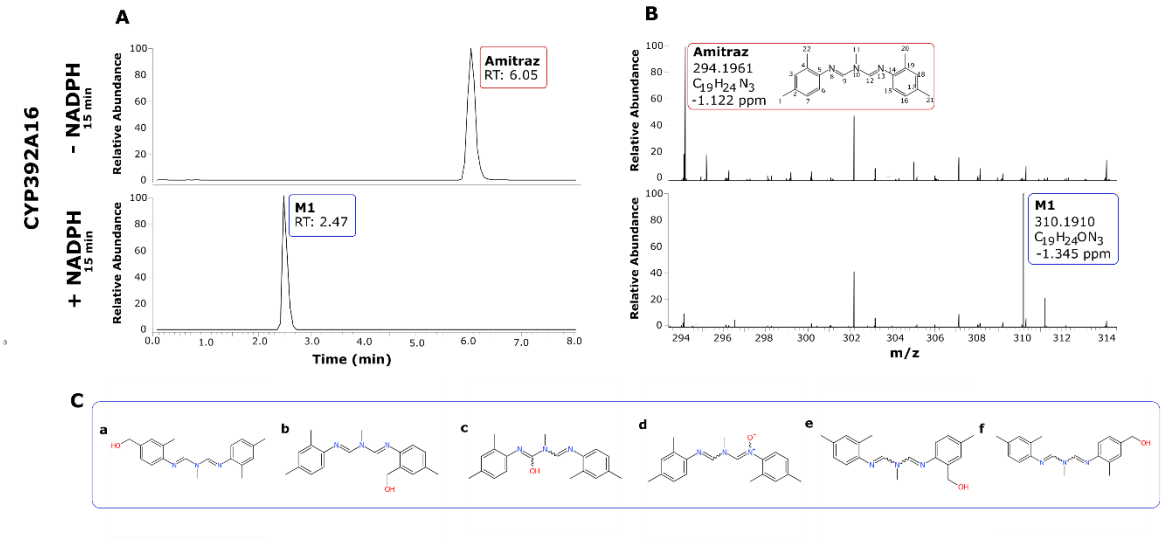

1366

1367 **Figure 4**. **CYP392A16 metabolism of the acaricide amitraz.** A) HPLC extracted ion
1368 chromatograms obtained using high resolution full scan MS show that CYP392A16 causes a
1369 NADPH-dependent transformation of amitraz (eluting at 6.05 min) to a metabolite M1 (eluting
1370 at 2.47 min). B) Accurate mass spectra obtained using HPLC - electrospray ionization. Upper
1371 panel: High-resolution accurate mass of protonated amitraz at m/z 294.1961. Lower panel:
1372 High-resolution accurate mass of the protonated amitraz metabolite M1 at m/z 310.1910.
1373 Shown with their assigned elemental composition and corresponding mass accuracy. C)
1374 Possible structures of the hydroxylated metabolite of amitraz, with according the Bio
1375 Transformer 3.0 tool several hydroxylation sites being possible.

1376

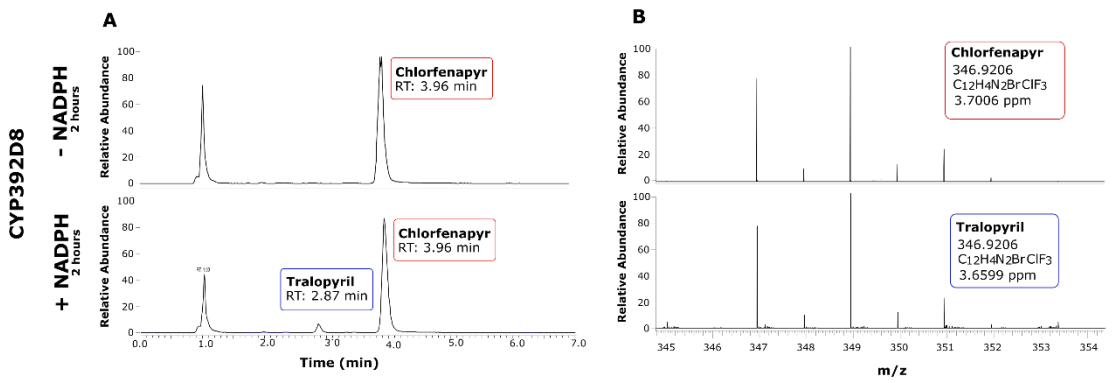

1377

1378 **Figure 5**. **CYP392D8 activation of the pro-acaricide chlorfenapyr to tralopyril.** A) HPLC
1379 extracted ion chromatograms obtained using high resolution full scan MS, show that
1380 CYP392D8 causes a NADPH-dependent transformation of chlorfenapyr (eluting at 3.96 min)
1381 to its toxic metabolite, tralopyril (eluting at 2.87 min). B) Accurate mass spectra obtained using
1382 HPLC - electrospray ionization. Upper panel: High-resolution accurate mass of chlorfenapyr.
1383 Lower panel: High-resolution accurate mass of the toxic metabolite of chlorfenapyr, tralopyril.
1384 Chlorfenapyr and tralopyril were detected in negative ion mode, and not in the protonated
1385 molecular ion form, due to the loss of the N-ethoxymethyl group, when introduced in the ESI
1386 source.

1387

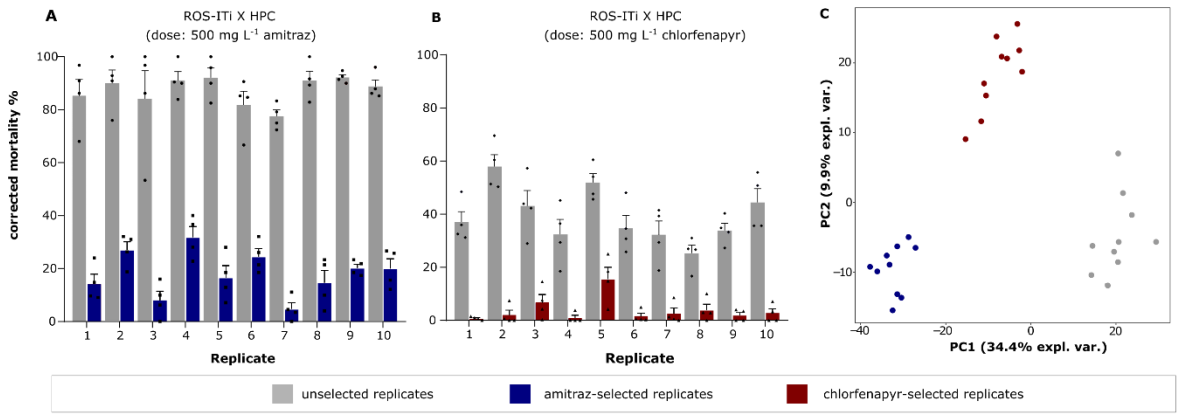

1388

1389 **Figure 6. Phenotypic and genomic differentiation after amitraz and chlorfenapyr selection.**
1390 A) Adult corrected mortality of long-term selected and control (unselected) populations after
1391 application of 500 mg L^{-1} amitraz. B) Adult corrected mortality of long-term selected and
1392 control (unselected) populations after application of 500 mg L^{-1} chlorfenapyr. C) Principal
1393 component analysis (PCA) of the unselected and selected populations of ROS-ITi X HPC cross
1394 based on genome-wide allele frequencies at polymorphic sites. The PCA clearly separates the
1395 amitraz-selected from the chlorfenapyr-selected and unselected populations.

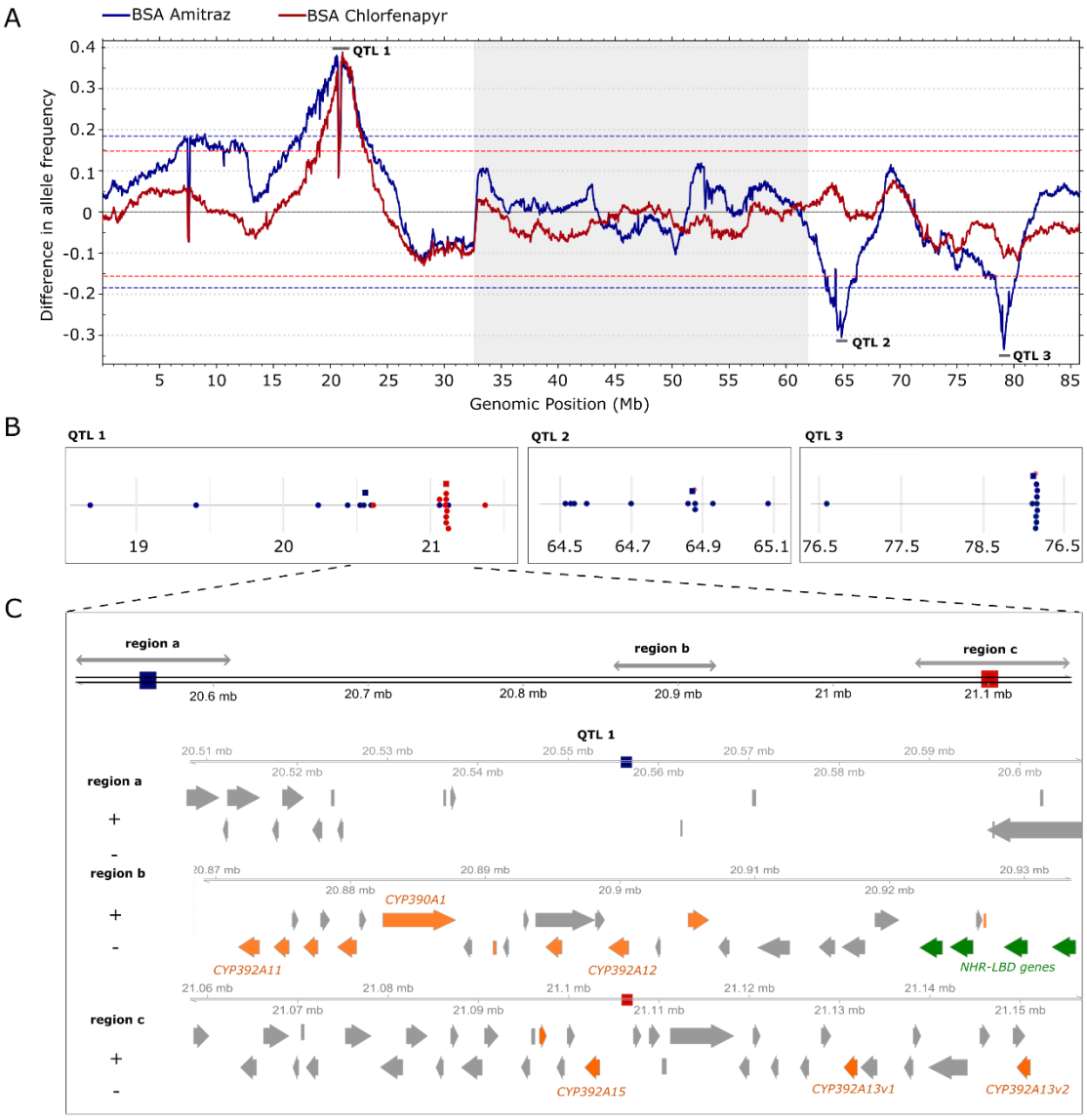

Figure 7. Genomic responses to amitraz and chlorfenapyr selection in the chlorfenayr selected strain (HPC) based QTL mapping. A) Averaged genome-wide change in allele frequency using ten chlorfenapyr selected sub-populations (red) and ten amitraz selected sub-populations (blue) compared to their paired unselected controls, originating from HPC. Dashed red (chlorfenapyr) and blue (amitraz) lines delineate statistical significance for QTL detection (FDR of 5%). For both QTL mapping experiments, one mutual QTL on chromosome 1 exceeded the 5% FDR threshold; QTL1 at ~20.85 Mb. For the amitraz two extra downward facing QTLs on chromosome 3 were detected that exceeded the 5% FDR threshold; QTL2 at ~3.008 Mb and QTL3 at ~17.263 Mb. Chromosomes are ordered by decreasing length and are indicated by alternating shading. B) Chromosome location of QTL1 peaks (left), QTL2 peaks (middle) and QTL3 peaks (right) for each replicate of BSA chlorfenapyr (red) and BSA amitraz

(blue). Chromosome location of average of each QTL peak calculated by combining all replicates into a single analysis (see panel A) are indicated with a solid square, while QTL peaks of single replicates are indicated with a solid circle. C) graphical representation of genes within interesting regions of QTL1. Regions A and C represent a 50 kb window surrounding the QTL1 peak maximum of the amitraz and chlorfenapyr BSA, respectively. Region B, on the other hand, is a region located around 20.9 Mb which contains a cluster of P450 genes and pseudogenes (highlighted in orange) and a cluster of HR96-LBD genes (highlighted in green).

Supplementary Figures

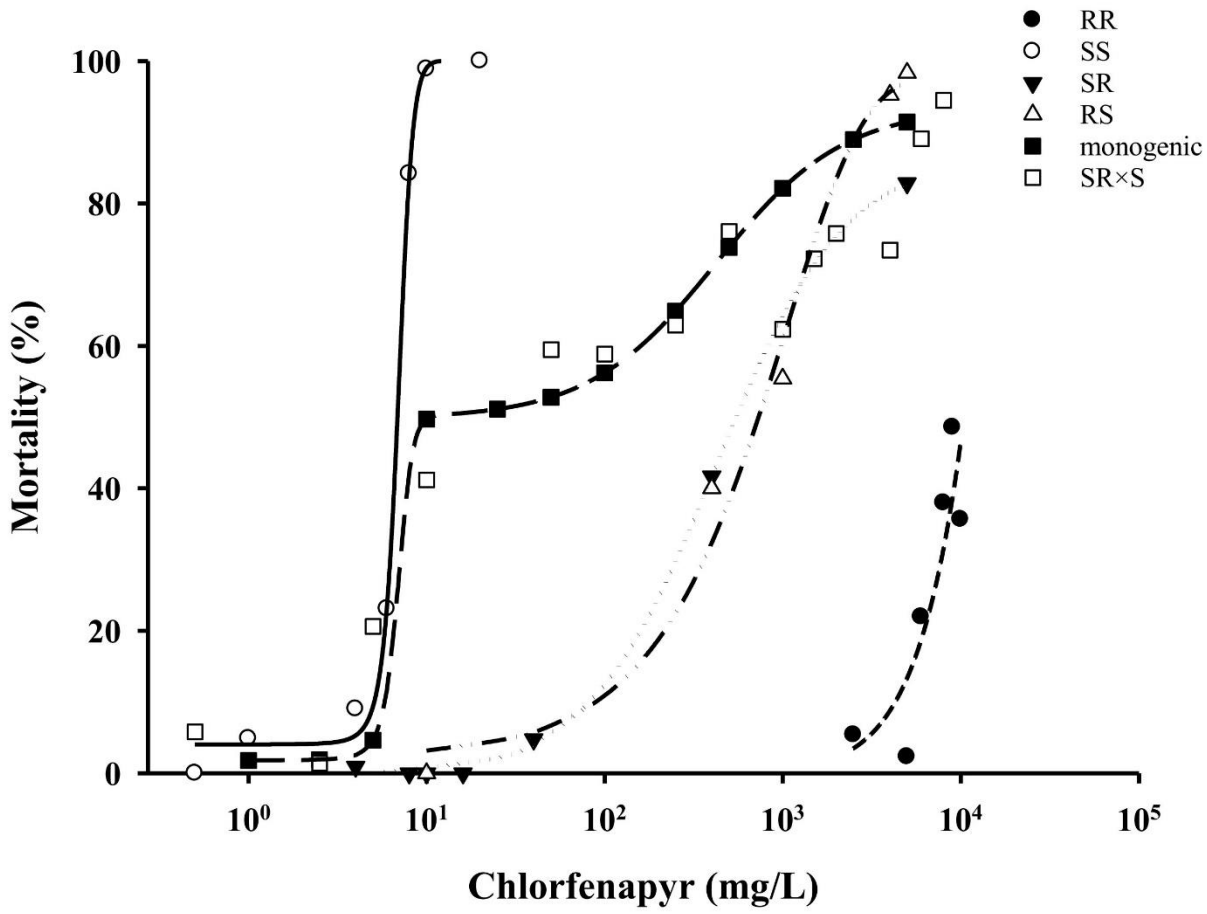

Supplementary Figure 1: Chlorfenapyr has as monogenic basis in HPC. Concentration-mortality curves for chlorfenapyr in strains HPC (•) , LON (○), the reciprocal crosses HPC x LON (▼) and LON x HPC (△), the (LON x HPC)F1 x LON backcross (☐) and the theoretical backcross based on monogenic inheritance (■)

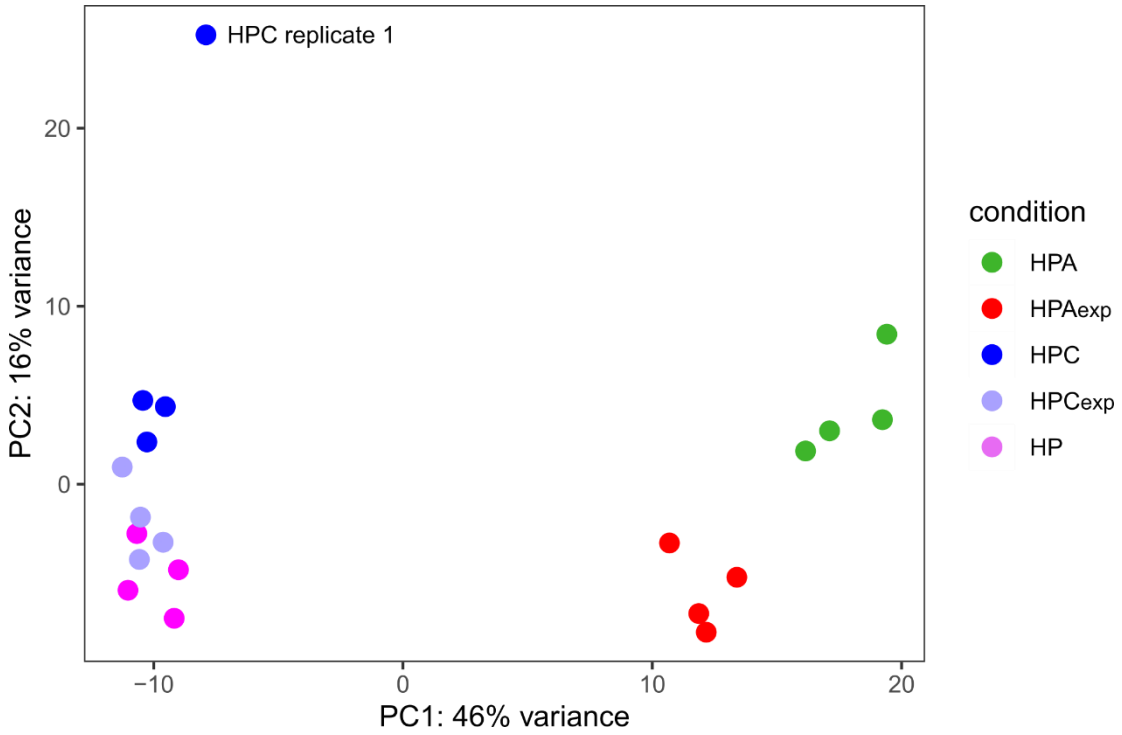

Supplementary Figure 2. Principal component analysis (PCA) to identify the outlier in the dataset. PCA based on transcriptional differences within and between HP and the derived laboratory-selected amitraz- or chlorfenapyr resistant subpopulations (HPA/HPAexp and HPC/HPCexp, respectively) identifying HPC replicate 1 to be an outlier and thus to be excluded from all further transcriptomic analysis. PC1 and PC2 are presented on the x- and y-axis respectively, with the percentage of variance explained by each PC shown in parenthesis.

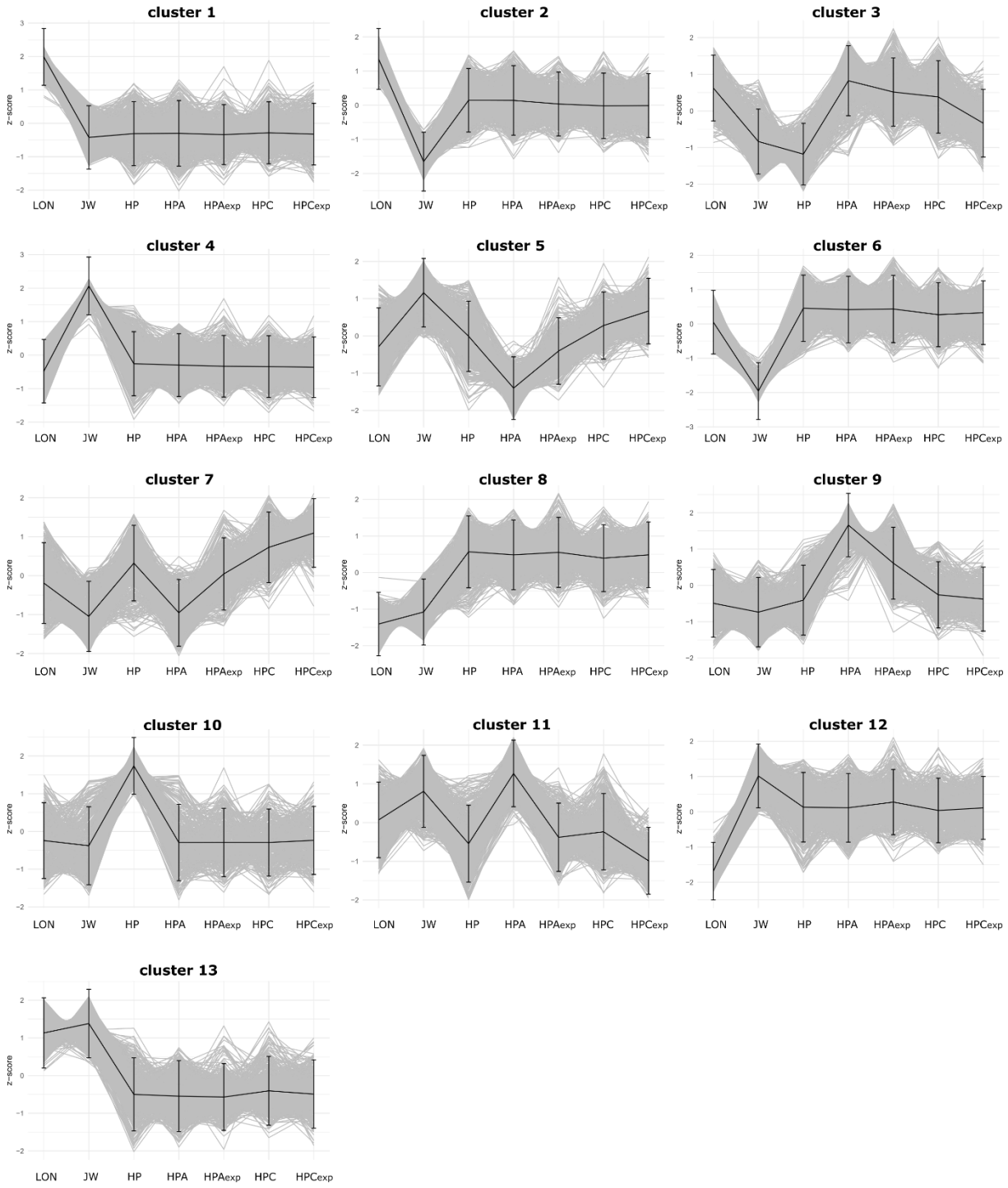

Supplementary Figure 3. Z-scores of all genes within each cluster of *T. urticae* strains LON, JW, HP, HPA, HPAexp, HPC and HPCexp. For each cluster, plots were made representing the average z-score for all replicates per treatment group per gene in the cluster (grey lines), which was thereafter used to calculate the average z-score trend (black line) with standard deviation across all genes in the cluster.

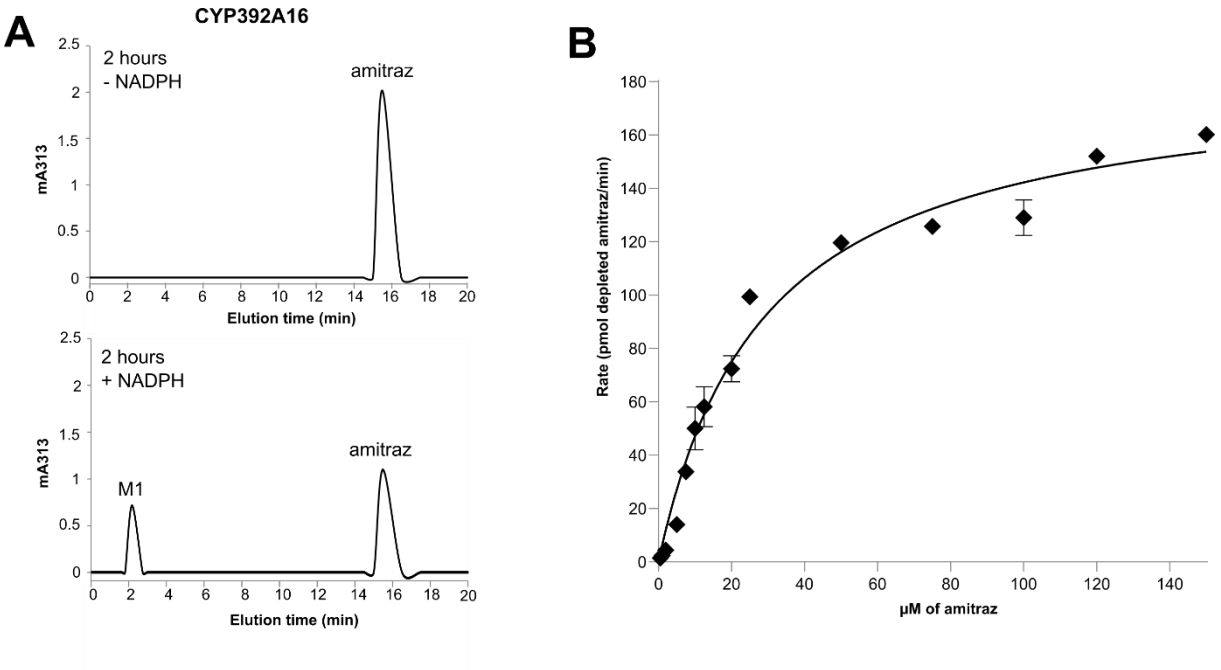

Supplementary Figure 4. CYP392A16 activity towards the acaricide amitraz. A) HPLC chromatograms show a NADPH-dependent depletion of the acaricide amitraz (eluting at 15.4 min) and the corresponding formation of an unknown metabolite (eluting at 2.17 min). Absorbance curves are plotted in blue. B) Michaelis–Menten kinetics of the depletion of amitraz by CYP392A16. Plotted values represent the mean. The curve was calculated by non-linear regression.

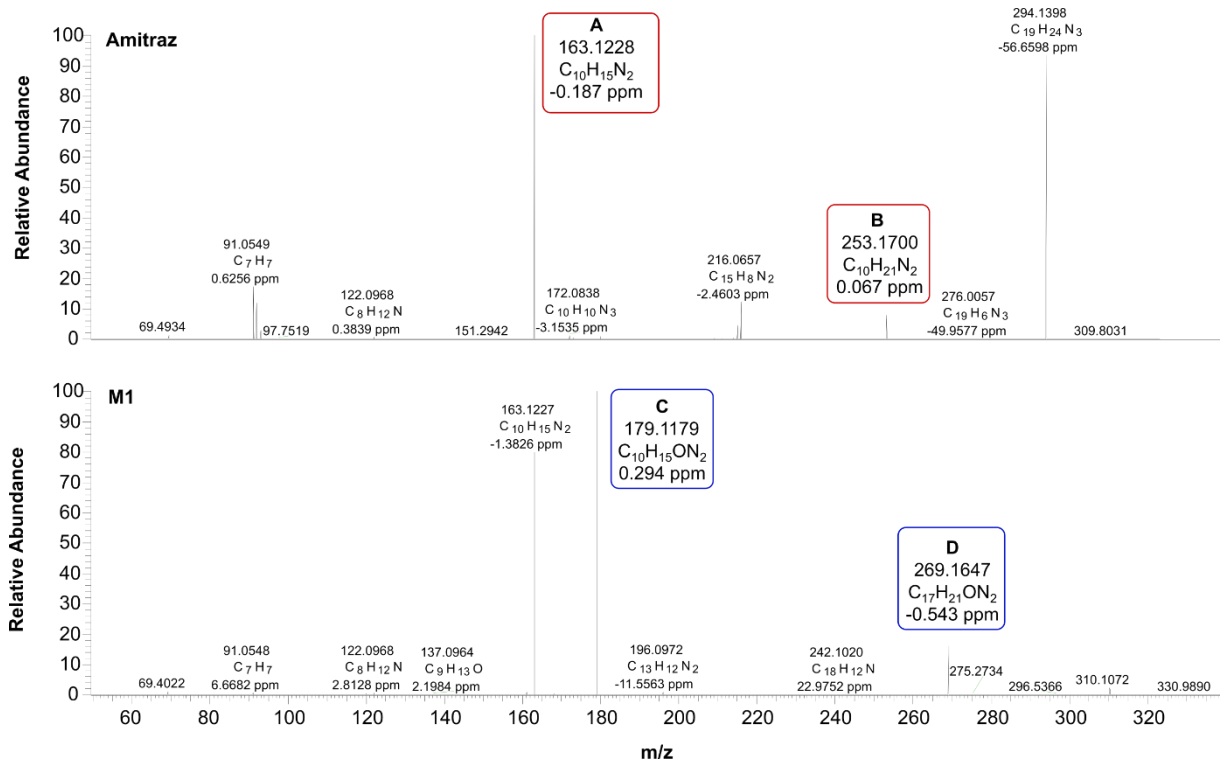

Supplementary Figure 5. Parallel reaction monitoring of the protonated amitraz (upper panel) and its metabolite, M1, proposed to be hydroxyl-amitraz, (lower panel). The product ions for amitraz precursor ions; A) m/z 163.1228 and B) m/z 253.1700 and product ions of metabolite M1 precursor ions C) m/z 179.1179 and D) m/z 269.1647. occur a mass difference of +15.99 Da between the parental amitraz and its metabolite M1. This is reflected in the amitraz (A and B) and M1 metabolite (C and D) product ions formed by collision induced dissociation as they have a 15.99 Da difference (A $\xrightarrow{+15.99}$ C, B $\xrightarrow{+15.99}$ D) , supporting that hydroxylation as the main mechanism.

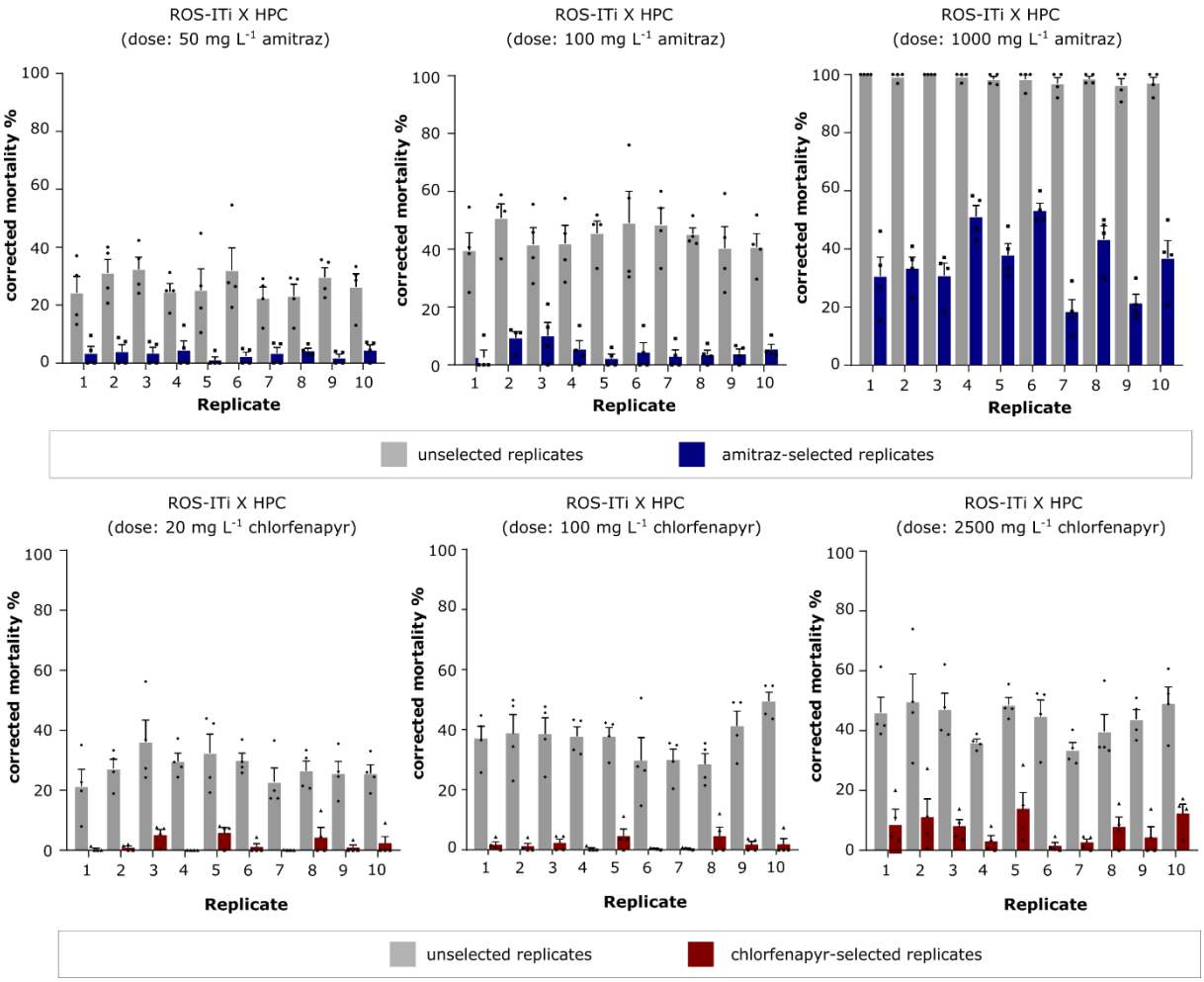

Supplementary Figure 6. Phenotypic response after amitraz and chlorfenapyr selection. Other doses tested than Figure 6A. Adult corrected mortality of long-term selected and control (unselected) populations after application of 50, 100 or 1000 mg L^{-1} amitraz or 10, 100 and 2500 mg L^{-1} chlorfenapyr.

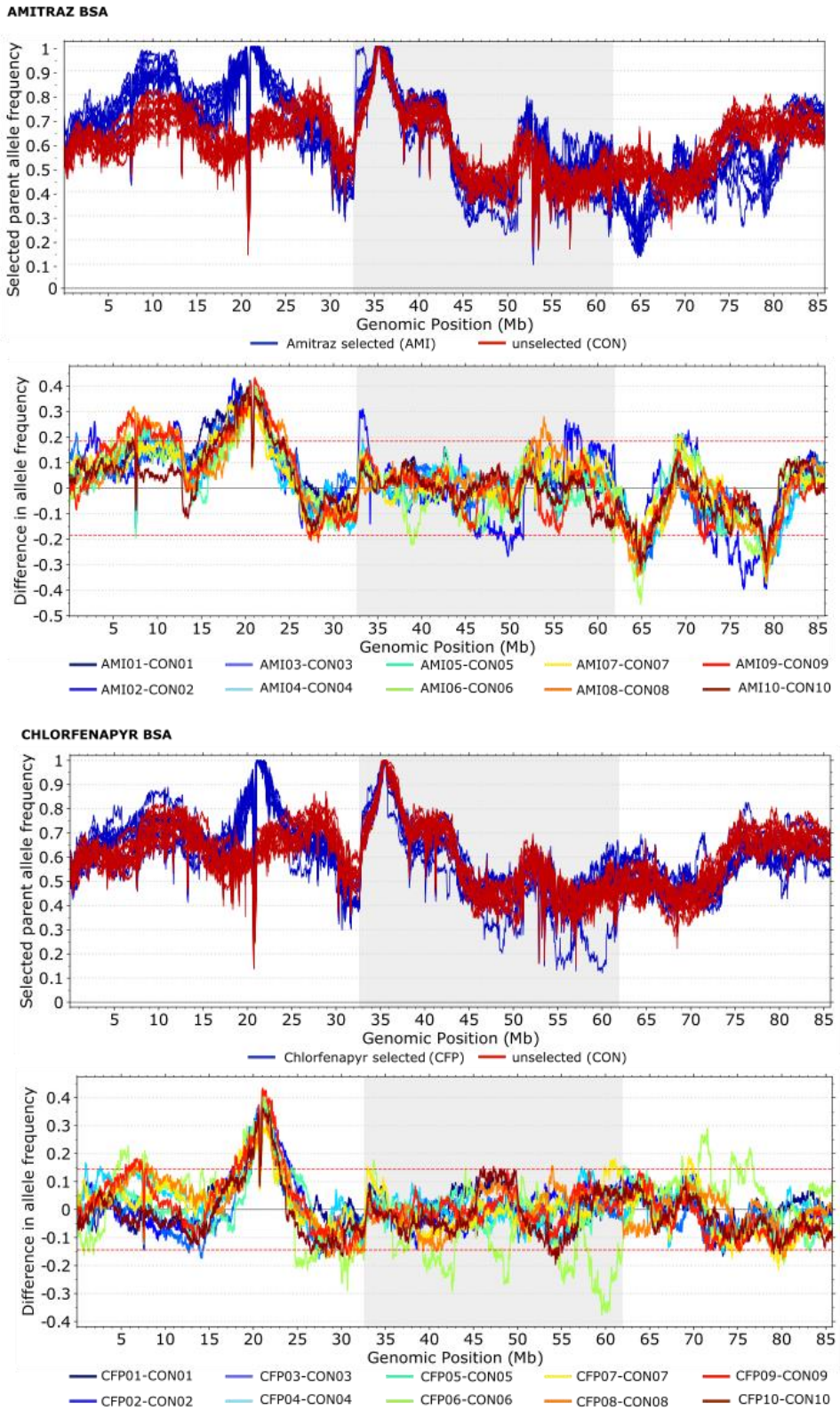

Supplementary Figure 7. BSA allele frequencies of individual replicates. Deviations in allele frequencies of amitraz selected (AMI), chlorfenapyr selected (CFP) and unselected (control, CON) populations of BSA amitraz and BSA chlorfenapyr.

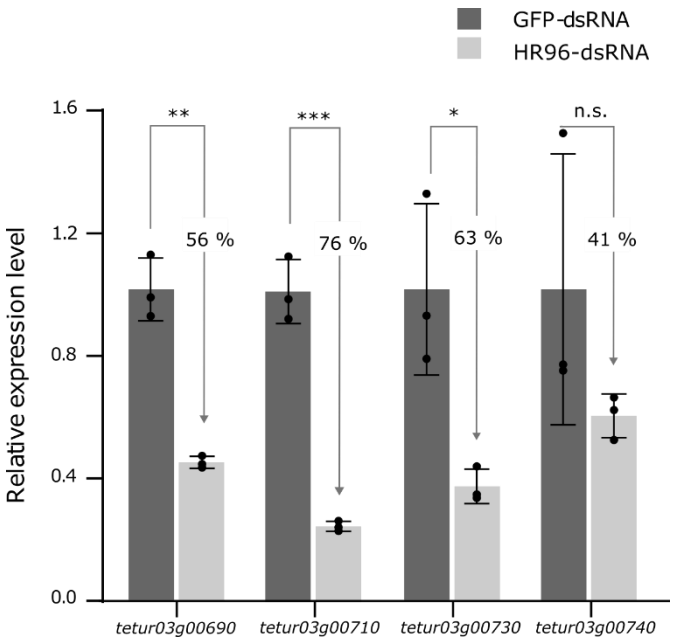

Supplementary Figure 8. Silencing efficiency of HR96-LDB cluster after RNAi. Relative expression levels of the HR96-LBD cluster (*tetur03g00690*, *tetur03g00710*, *tetur03g00730* and *tetur03g00740)* determined by RT-qPCR after injection with HR96-dsRNA or GFP-dsRNA as a control. Expression levels are scaled to the mean of the control in each experiment. For the bar plot, means (n=3), error bars of ±1 standard deviation, and all data points are shown. Statistical insignificances were observed using t-tests with Benjamini-Hochberg correction (n.s., not significant; p adj < 0.05*, p adj < 0.01**, and p adj < 0.001***).

Supplementary Table Information

Supplementary Table 1. Primers used for RT-qPCR for genes listed in column "Target" and amplification of products for use in dsRNA production against HR96-LBD genes and GFP (column "Target"). In the primer sequences (columns "Sequence Fw (5'-3')" and "Sequence Fw (5'-3')"), lowercase letters are the T7 promoter sequence used for in vitro transcription. The respective primer Tm values and the product lengths are provided in columns "Fw Tm (°C)", "Rv Tm (°C)", and "Product size (bp)".

Supplementary Table 2. Observed and expected values of mortality in the backcross ((LON ♀ × HPC ♂)♀ x LON ♂) made to determine the chlorfenapyr mode of inheritance, together with the corresponding X^2 for the monogenic inheritance hypothesis. Expected mortality calculated via formula of Georgiou $c = (0.5)\ W_{\text{LON x HPC}} + (0.5)\ W_{\text{LON}}$, where c is the expected mortality at each given concentration and W is the observed mortality of the F_1 LON x HPC and parental LON genotypes at each given concentration. LC_{50}s of SR and RS populations together with the dominance values (D values).

Supplementary Table 3. Number of generated strand-specific paired-end Illumina reads and their mapping rates against the *Tetranychus urticae* 3 chromosome assembly for all sample groups.

Supplementary Table 4. Gene ID's of all genes that show significant differences in expression across all samples based on z-scaled normalized read-counts (p value < 0.001 as determined by LTR test), grouped into 13 clusters with the k-means clustering algorithm.

Supplementary Table 5. Enriched GO terms per cluster.

Supplementary Table 6. Differentially expressed genes (DEGs, absolute Log_2 Fold Change ($|Log_2FC| > 1$, p adj < 0.05) in all pairwise comparisons between LON, JW, HP, HPA, HPAexp, HPC and HPCexp. For each comparison, Log_2 fold change (Log_2FC), standard error for Log_2FC, and adjusted p values for each gene are provided in columns "Log2FC", "lfcSE", and "p adj", respectively.

Supplementary Table 7. Numbers of differentially expressed genes in different comparisons between LON, JW, HP, HPA, HPAexp, HPC and HPCexp. Upregulated genes are DEGs with $Log_2FC > 1$, downregulated genes are DEGs with $Log_2FC < -1$.

Supplementary Table 8. Cytochrome P450 genes per cluster.

Supplementary Table 9. Yields of *T. urticae* P450s expressed in *E. coli* with their characteristic CO-reduced spectrum.

Supplementary Table 10. Genes located at genomic window of each QTL. For QTL1 (~20.850 Mb on chromosome 1) genes from 100 kb downstream of the amitraz BSA average (~20.558 Mb; indicated in blue shading) to 100 kb upstream of the chlorfenapyr BSA average (~21.108 Mb; indicated in red shading). For QTL2 and QTL3 genes in a 100 kb bracket of the amitraz BSA average (~3.008 Mb and ~17.263 Mb on chromosome 3, respectively; indicated in blue shading). Log_2FC of DEGs between parental strains HPC and ROS-ITi are shown, with n.s. meaning not significant (p adj > 0.05). For QTL 1 AA mutations enriched in selected samples are shown for both BSA experiments.

Supplementary Table 11. : Output of DESeq2 for pairwise comparisons to identify differentially expressed genes between mites injected with dsHR96 (treatment) versus dsGFP (control). Here, all genes with p value < 0.05 are presented. For each comparison, Log_2 fold change (Log_2FC), standard error for Log_2FC, and adjusted p values for each gene are provided in columns “log2FC”, “lfcSE”, and “p adj”, respectively.

1523